Synchronized Oscillatory Dynamics for a 1-D Model of Membrane Kinetics Coupled by Linear Bulk Diffusion

J. GOU, Y. X. L I, W. NAGATA, M. J. WARD

Department of Mathematics, University of British Columbia, Vancouver, British Columbia, V6T 1Z2, Canada,

(*Received 4 September 2015*)

Spatio-temporal dynamics associated with a class of coupled membrane-bulk PDE-ODE models in one spatial dimension is analyzed using a combination of linear stability theory, numerical bifurcation software, and full time-dependent simulations. In our simplified 1-D setting, the mathematical model consists of two dynamically active membranes, separated spatially by a distance $2L$, that are coupled together through a linear bulk diffusion field, with a fixed bulk decay rate. The coupling of the bulk and active membranes arises through both nonlinear flux boundary conditions for the bulk diffusion field together with feedback terms, depending on the local bulk concentration, to the dynamics on each membrane. For this class of models, it is shown both analytically and numerically that bulk diffusion can trigger a synchronous oscillatory instability in the temporal dynamics associated with the two active membranes. For the case of a single active component on each membrane, and in the limit $L \to \infty$, rigorous spectral results for the linearization around a steady-state solution, characterizing the possibility of Hopf bifurcations and temporal oscillations in the membranes, are obtained. For finite L, a weakly nonlinear theory, accounting for eigenvalue-dependent boundary conditions appearing in the linearization, is developed to predict the local branching behavior near the Hopf bifurcation point. The analytical theory, together with numerical bifurcation results and full numerical simulations of the PDE-ODE system, are undertaken for various coupled membrane-bulk systems, including two specific biologically relevant applications. Our results show the existence of a wide parameter range where stable synchronous oscillatory dynamics in the two membranes can occur.

Key words: membrane dynamics, bulk diffusion, Hopf bifurcation, winding number, synchronous oscillations, weakly nonlinear analysis, amplitude equation.

1 Introduction

In this paper we explore a new modeling paradigm for the synchronization or collective dynamics of spatially segregated, but dynamically active, localized regions that are coupled spatially through a linear diffusion field. For the resulting class of PDE-ODE models, spatial-temporal dynamics will be analyzed using a combination of linear stability theory, numerical bifurcation software, and full time-dependent simulations. Our analysis will show that such a coupling by a linear diffusion field is a robust mechanism for the initiation of synchronized oscillatory dynamics in the segregated compartments.

Coupled membrane-bulk dynamics, or the coupling of dynamically active spatially segregated compartments through a linear bulk diffusion field, arises in many applications including, models of biological quorum sensing behavior (cf. [**3**], [**21**]), models of the multistage adsorption of viral particles trafficking across biological membranes (cf. [**4**]), Turing patterns resulting from coupled bulk and surface diffusion (cf. [**17**]), and models of the effect of catalyst particles on chemically active surfaces (cf. [**28**]). For one such model, it was shown numerically in [**10**] that a two-component membrane-bulk dynamics on a 1-D spatial domain can trigger synchronous oscillatory dynamics in the two membranes. In the context of cellular signal transduction, the survey [**14**] emphasizes the need for developing more elaborate models of cell signaling that are not strictly ODE based, but that, instead, involve spatial diffusion processes coupled with kinetics arising from localized signaling compartments.

A related class of models, referred to here as quasi-static models, consist of linear bulk diffusion fields that are coupled

solely through nonlinear fluxes defined at specific spatial lattice sites. Such systems arise in the modeling of signal cascades in cellular signal transduction (cf. [**18**]), and in the study of the effect of catalyst particles and defects on chemically active substrates (cf. [**25**], [**22**]). In [**22**] it was shown numerically that one such quasi-static model exhibits an intricate spatial-temporal dynamics consisting of a period-doubling route to chaotic dynamics.

Motivated by these prior studies, the goal of this paper is to formulate and analyze a general class of coupled membrane-bulk dynamics in a simplified 1-D spatial domain. In our simplified 1-D setting, we assume that there are two dynamically active membranes, located at $x = 0$ and $x = 2L$, that can release a specific signaling molecule into the bulk region $0 < x < 2L$, and that this secretion is regulated by both the bulk concentration of that molecule together with its concentration on the membrane. In the bulk region, we assume that the signaling molecule undergoes passive diffusion with a specified bulk decay rate. If $C(x,t)$ is the concentration of the signaling molecule in the bulk, then its spatial-temporal evolution in this region is governed by the dimensionless model

$$\begin{aligned} \tau C_t = DC_{xx} - C\,, \qquad t>0\,, \quad 0<x<2L\,, \\ DC_x(0,t) = G(C(0,t),u_1(t))\,, \qquad -DC_x(2L,t) = G(C(2L,t),v_1(t))\,, \end{aligned} \tag{1.1 a}$$

where $\tau > 0$ is a time-scale for the bulk decay and $D/\tau > 0$ is the constant diffusivity. On the membranes $x = 0$ and $x = 2L$, the fluxes $G(C(0,t),u_1)$ and $G(C(2L,t),v_1)$ model the influx of signaling molecule into the bulk, which depends on the bulk concentrations $C(0,t)$ and $C(2L,t)$ at the two membranes together with the local concentrations $u_1(t)$ and $v_1(t)$ of the signaling molecule on the membranes. We assume that on each membrane, there are n species that can interact, and that their dynamics are described by n-ODE's of the form

$$\frac{d\boldsymbol{u}}{dt} = \boldsymbol{\mathcal{F}}(\boldsymbol{u}) + \beta\mathcal{P}(C(0,t),u_1)\boldsymbol{e_1}\,, \qquad \frac{d\boldsymbol{v}}{dt} = \boldsymbol{\mathcal{F}}(\boldsymbol{v}) + \beta\mathcal{P}(C(2L,t),v_1)\boldsymbol{e_1}\,, \tag{1.1 b}$$

where $\boldsymbol{e}_1 \equiv (1,0,\ldots,0)^T$. Here, $\boldsymbol{u}(t) \equiv (u_1(t),\ldots,u_n(t))^T$ and $\boldsymbol{v}(t) \equiv (v_1(t),\ldots,v_n(t))^T$ is the concentration of the n species on the two membranes and $\boldsymbol{\mathcal{F}}(\boldsymbol{u})$ is the vector nonlinearity modeling the chemical kinetics for these membrane-bound species. In our formulation (1.1 b), only one of these internal species, labeled by u_1 and v_1 at the two membranes, is capable of diffusing into the bulk. The coupling to the bulk is modeled by the two feedback terms $\beta\mathcal{P}(C(0,t),u_1)$ and $\beta\mathcal{P}(C(2L,t),v_1)$, where the coupling parameter β models the strength of the membrane-bulk exchange. In Fig. 1 we give a schematic plot of the geometry for (1.1).

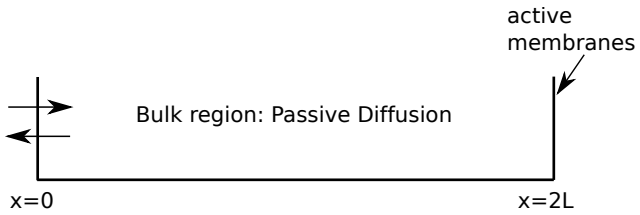

Figure 1. Schematic plot of the geometry for (1.1) showing the bulk region $0 < x < 2L$, where passive diffusion occurs, and the two dynamically active membranes at $x = 0$ and $x = 2L$. One of the membrane species can be exchanged between the membrane and the bulk.

In §2 we construct a steady-state solution for (1.1) that is symmetric about the midline $x = L$. The analytical construction of this symmetric steady-state solution is reduced to the problem of determining roots to a nonlinear algebraic system involving both the local membrane kinetics and the nonlinear feedback and flux functions. We then formulate the linear stability problem associated with this steady-state solution. In our stability theory, we must allow for perturbations that are either symmetric or anti-symmetric about the midline, which leads to the possibility of either synchronous (in-phase) or asynchronous (out-of-phase) instabilities in the two membranes. By using a matrix determinant lemma for rank-one

perturbations of a matrix, we show that the eigenvalue parameter associated with the linearization around the steady-state satisfies a rather simple transcendental equation for either the synchronous or asynchronous mode.

In §3 we analyze in detail the spectrum of the linearized problem associated with a one-component membrane dynamics. For the infinite-line problem, corresponding to the limit $L \to +\infty$, in §3.1 we use complex analysis together with a rigorous winding number criterion to derive sufficient conditions, in terms of properties of the reaction-kinetics and nonlinear feedback and flux, that delineate parameter ranges where Hopf bifurcations due to coupled membrane-bulk dynamics will occur. Explicit formulae for the Hopf bifurcation values, in terms of critical values of τ in (1.1), are also obtained. In §3.1 further rigorous results are derived that establish parameter ranges where no membrane oscillations are possible. For the finite-domain problem, and assuming a one-component membrane dynamics, we show in §3.2 that some of the rigorous results for the infinite-line problem, as derived in §3.1, are still valid. However, in general, for the finite-domain problem numerical computations of the winding number are needed to predict Hopf bifurcation points and to establish parameter ranges where the steady-state solution is linearly stable.

We remark that for the case of a one-component membrane dynamics, the eigenvalue problem derived in §3.1, characterizing the linear stability of the coupled membrane-bulk dynamics, is remarkably similar in form to the spectral problem that arises in the stability of localized spike solutions to reaction-diffusion (RD) systems of activator-inhibitor type (cf. [**23**] and [**29**] and the references therein). More specifically, on the infinite-line, the spectral problem for our coupled membrane-bulk dynamics is similar to that studied in §3.1 of [**23**] for a class of activator-inhibitor RD systems.

For a one-component membrane dynamics, in §4 we illustrate the theory of §3 for determining Hopf bifurcation points corresponding to the onset of either synchronous or asynchronous oscillatory instabilities. For the infinite-line problem, where these two instability thresholds have coalesced to a common value, we illustrate the theoretical results of §3.1 for the existence of a Hopf bifurcation point. For the finite-domain problem, where the two active membranes are separated by a finite distance $2L$, numerical computations of the winding-number are used to characterize the onset of either mode of instability. The theory is illustrated for a class of feedback models in §4.1, for an exactly solvable model problem in §4.2, and for two specific biological systems in §4.3. The biological systems in §4.3 consist of a model of hormonal activity due to GnRH neurons in the hypothalamus (cf. [**13**], [**19**], and [**7**]), and a model of quorum sensing behavior of *Dictyostelium* (cf. [**9**]). For the problems in §4.1–4.3, we supplement our analytical theory with numerical bifurcation results, computed from the coupled membrane-bulk PDE-ODE system using the bifurcation software XPPAUT [**6**]. For the *Dictyostelium* model and the model in §4.2, our results shows that there is a rather large parameter range where stable synchronous membrane oscillations occur. Full numerical computations of the PDE-ODE system of coupled membrane-bulk dynamics, undertaken using a method-of-lines approach, are used to validate the theoretical predictions of stable synchronous oscillations.

In §5 we consider a specific coupled membrane-bulk model having two active components on each membrane. To enhance the relevance of our coupled model, the dynamics on the membrane are taken from the seminal survey of [**24**], which characterizes some key design principles for realistic biological oscillators. For the case where the two membranes are identical, and have a common value of the coupling strength to the bulk medium, we use a numerical winding number argument to predict the onset of either a synchronous or an asynchronous oscillatory solution branch that bifurcates from the steady-state solution. The numerical bifurcation package XPPAUT [**6**] shows that there is a parameter range where the synchronous solution branch exhibits bistable behavior. In contrast, in the heterogeneous case where the coupling strengths to the two membranes are different, we show that the amplitude ratio of the oscillations in the two membranes can be very large, with one membrane remaining, essentially, in a quiescent state.

For the case of a one-component membrane dynamics on a finite domain, in §6 we formulate and then implement a weakly nonlinear multiple time-scale theory to derive an amplitude equation that characterizes whether a synchronous oscillatory instability is subcritical or supercritical near the Hopf bifurcation point. For a specific choice of the nonlinearities, corresponding to the model considered in §4.2, theoretical predictions based on the amplitude equation are then confirmed with full bifurcation results computed using XPPAUT (cf. [**6**]).

The key theoretical challenge and novelty of our weakly nonlinear analysis in §6 is that both the differential operator and the boundary condition on the membrane for the linearized problem involves the eigenvalue parameter. This underlying spectral problem, with an eigenvalue-dependent boundary condition, is not self-adjoint and is rather non-standard. Motivated by the theoretical approach developed in [**8**] to account for eigenvalue-dependent boundary conditions, we introduce an extended operator $\mathcal{L}$, and an associated inner product, from which we determine the corresponding adjoint problem. In this way, we formulate an appropriate solvability condition in Lemma 6.1 that is one of the key ingredients, in our multiple time-scale analysis, for deriving the amplitude equation characterizing the branching behavior of synchronous oscillations near onset. We remark that a similar methodology of introducing an extended operator to treat a transcritical bifurcation problem involving an eigenvalue-dependent boundary condition, which arises in a mathematical model of thermoelastic contact of disc brakes, was undertaken in [**26**] and [**27**]. However, to our knowledge, there has been no previous work for the corresponding Hopf bifurcation problem of the type considered herein.

Finally, we remark that, as far as we are aware, there has been rather little work in the mathematical literature on membrane-bulk interactions. Several open problems in this area that warrant further investigation are discussed briefly in §7. Additional recent studies of the effect of membrane-bulk coupling for certain two-component membrane dynamics are given in [**11**] and in [**12**]. With the exception of the general formulation of the model in §2 and the specific example considered in §5, this paper has focused on developing mathematical theory for membrane-bulk interactions with one-component membrane dynamics. In [**11**], an asymptotic analysis of membrane-bulk oscillations is given for the specific model of [**10**] with slow-fast Fitzhugh-Nagumo membrane kinetics. By exploiting the asymptotic limit of the slow-fast structure, a phase diagram in parameter space where synchronous and asynchronous oscillations occur can, essentially, be determined analytically by calculating the winding number associated with the linearized problem in the slow-fast limit. In §5 of this paper, such a reduction was not possible for our only example of two-component dynamics, where the winding number had to be computed numerically. In [**12**], membrane-bulk oscillations for a 2-component membrane dynamics with Selkov kinetics is analyzed. The primary focus of [**12**] is to develop a weakly nonlinear theory to study oscillations near a co-dimension-two Torus bifurcation point corresponding to a special parameter set where each of the synchronous and asynchronous branches of oscillations exhibit an exchange of stability.

2 The Steady-State Solution and the Formulation of the Linear Stability Problem

In this section we construct a steady-state solution for (1.1), and then formulate the associated linear stability problem. In (1.1), we have assumed for simplicity that the two membranes have the same kinetics and membrane-bulk coupling mechanisms. As such, this motivates the construction of a steady-state solution for (1.1) that is symmetric with respect to the midline $x = L$ of the bulk region. The corresponding symmetric steady-state bulk solution $C_e(x)$ and the membrane-bound steady-state concentration field $\boldsymbol{u}_e$ satisfy

$$\begin{aligned} &D\partial_{xx}C_e - C_e = 0\,, \qquad 0 < x < L\,; \qquad \partial_x C_e(L) = 0\,, \quad D\partial_x C_e(0) = G\left(C_e(0), u_{1e}\right)\,, \\ &\boldsymbol{\mathcal{F}}(\boldsymbol{u}_e) + \beta\mathcal{P}(C_e(0), u_{1e})\boldsymbol{e_1} = 0\,. \end{aligned} \tag{2.1}$$

We readily calculate that

$$C_e(x) = C_e^0 \frac{\cosh\left[\omega_0(L-x)\right]}{\cosh(\omega_0 L)}\,, \qquad \omega_0 \equiv 1/\sqrt{D}\,, \tag{2.2 a}$$

where $C_e^0 \equiv C_e(0)$ and $\boldsymbol{u}_e$ are the solutions to the $n+1$ dimensional nonlinear algebraic system

$$-C_e^0 \tanh(\omega_0 L) = \omega_0 G\left(C_e^0, u_{1e}\right)\,, \qquad \boldsymbol{\mathcal{F}}(\boldsymbol{u}_e) + \beta \mathcal{P}(C_e^0, u_{1e})\boldsymbol{e_1} = 0\,. \tag{2.2 b}$$

In general it is cumbersome to impose sufficient conditions on $\boldsymbol{\mathcal{F}}$, $\mathcal{P}$, and G, guaranteeing a solution to (2.2 *b*). Instead, we will analyze (2.2 *b*) for some specific models below in §4 and in §5.

To formulate the linear stability problem, we introduce the perturbation

$$C(x,t) = C_e(x) + e^{\lambda t}\eta(x)\,, \qquad \boldsymbol{u}(t) = \boldsymbol{u}_e + e^{\lambda t}\boldsymbol{\phi}\,,$$

into (1.1) and linearize. In this way, we obtain the eigenvalue problem

$$\begin{aligned} &\tau\lambda\eta = D\eta_{xx} - \eta\,, \qquad 0 < x < L\,; \qquad D\eta_x(0) = G_c^e\eta_0 + G_{u_1}^e\phi_1\,, \\ &J_e\boldsymbol{\phi} + \beta(\mathcal{P}_c^e\eta_0 + \mathcal{P}_{u_1}^e\phi_1)\boldsymbol{e}_1 = \lambda\boldsymbol{\phi}\,. \end{aligned} \tag{2.3}$$

Here we have defined $\eta_0 \equiv \eta(0)$, $G_c^e \equiv G_c(C_e^0, u_{1e})$, $G_{u_1}^e \equiv G_{u_1}(C_e^0, u_{1e})$, $\mathcal{P}_c^e \equiv \mathcal{P}_c(C_e^0, u_{1e})$, and $\mathcal{P}_{u_1}^e \equiv \mathcal{P}_{u_1}(C_e^0, u_{1e})$. In addition, J_e is the Jacobian matrix of the nonlinear membrane kinetics $\boldsymbol{\mathcal{F}}$ evaluated at $\boldsymbol{u}_e$.

The formulation of the linear stability problem is complete once we impose a boundary condition for η at the midline $x = L$. Due to the reflection symmetry of the spectral problem about the midline $x = L$, there are exactly two choices for this boundary condition for this linearized problem. The choice $\eta(L) = 0$ corresponds to an anti-phase synchronization of the two membranes (asymmetric case), while the choice $\eta_x(L) = 0$ corresponds to an in-phase synchronization of the two membranes. The goal of our analysis is to analyze whether there can be any Hopf bifurcations associated with either anti-phase or in-phase perturbations.

For the synchronous mode we solve (2.3) with $\eta_x(L) = 0$ to obtain that

$$\eta(x) = \eta_0 \frac{\cosh\left[\Omega_\lambda(L-x)\right]}{\cosh(\Omega_\lambda L)}\,, \qquad \Omega_\lambda \equiv \sqrt{\frac{1+\tau\lambda}{D}}\,, \tag{2.4}$$

where we have specified the principal branch of the square root if λ is complex. Upon substituting (2.4) into the boundary condition for η on $x = 0$ in (2.3), we readily determine η_0 in terms of ϕ_1 as

$$\eta_0 = -\frac{G_{u_1}^e\phi_1}{G_c^e + D\Omega_\lambda \tanh(\Omega_\lambda L)}\,. \tag{2.5}$$

We then substitute (2.5) into the last equation of (2.3), and rewrite the resulting expression in the form

$$(J_e - \lambda I)\,\boldsymbol{\phi} = p_+(\lambda)\phi_1\boldsymbol{e}_1\,, \qquad p_+(\lambda) \equiv \beta\left(\frac{G_{u_1}^e\mathcal{P}_c^e - \mathcal{P}_{u_1}^e G_c^e - \mathcal{P}_{u_1}^e D\Omega_\lambda \tanh(\Omega_\lambda L)}{G_c^e + D\Omega_\lambda \tanh(\Omega_\lambda L)}\right)\,. \tag{2.6}$$

Similarly, for the asynchronous mode we solve (2.3) with $\eta(L) = 0$ to get

$$\eta(x) = \eta_0 \frac{\sinh\left[\Omega_\lambda(L-x)\right]}{\sinh(\Omega_\lambda L)}\,.$$

Upon applying the boundary condition for η at $x = 0$ from (2.3), we can write η_0 in terms of ϕ_1 as

$$\eta_0 = -\frac{G_{u_1}^e\phi_1}{G_c^e + D\Omega_\lambda \coth(\Omega_\lambda L)}\,. \tag{2.7}$$

Upon substituting this expression into the last equation of (2.3), we can eliminate η_0 to obtain

$$(J_e - \lambda I)\,\boldsymbol{\phi} = p_-(\lambda)\phi_1\boldsymbol{e}_1\,, \qquad p_-(\lambda) \equiv \beta\left(\frac{G_{u_1}^e\mathcal{P}_c^e - \mathcal{P}_{u_1}^e G_c^e - \mathcal{P}_{u_1}^e D\Omega_\lambda \coth(\Omega_\lambda L)}{G_c^e + D\Omega_\lambda \coth(\Omega_\lambda L)}\right)\,. \tag{2.8}$$

In summary, we conclude that an eigenvalue λ and eigenvector $\boldsymbol{\phi}$ associated with the linear stability of the symmetric steady-state solution $(C_e(x),\, \boldsymbol{u}_e)$ is determined from the matrix system

$$(J_e - \lambda I - p_{\pm}(\lambda)E)\,\boldsymbol{\phi} = \mathbf{0}\,, \qquad E \equiv \boldsymbol{e}_1\boldsymbol{e}_1^T\,, \qquad \text{where} \qquad \boldsymbol{e}_1 \equiv (1,0,\ldots,0)^T\,. \tag{2.9}$$

Here $p_+(\lambda)$ and $p_-(\lambda)$ are defined for the synchronous and asynchronous modes by (2.6) and (2.8), respectively. We now seek values of λ for which (2.9) admits nontrivial solutions $\boldsymbol{\phi} \neq \mathbf{0}$. These values of λ satisfy the transcendental equation

$$\det\left(J_e - \lambda I - p_{\pm}(\lambda)E\right) = 0\,. \tag{2.10}$$

Since E is an $n\times n$ rank-one matrix, the transcendental equation (2.10) for the eigenvalue λ can be simplified considerably by using the following well-known Matrix Determinant Lemma:

Lemma 2.1 *Let A be an invertible $n \times n$ matrix and let $\boldsymbol{a}$ and $\boldsymbol{b}$ be two column vectors. Then,*

$$det\left(A + \boldsymbol{a}\boldsymbol{b}^T\right) = \left(1 + \boldsymbol{b}^T A^{-1}\boldsymbol{a}\right) det(A)\,. \tag{2.11}$$

Therefore, $(A + \boldsymbol{a}\boldsymbol{b}^T)\boldsymbol{\phi} = \mathbf{0}$ has a nontrivial solution if and only if $\boldsymbol{b}^T A^{-1}\boldsymbol{a} = -1$.

The proof of this result is straightforward and is omitted (see Lemma 1.1 of [**5**]). Applying this lemma to (2.10) and (2.9), where we identify $A \equiv J_e - \lambda I$, $\boldsymbol{a} \equiv -p_{\pm}\boldsymbol{e}_1$, and $\boldsymbol{b} \equiv \boldsymbol{e}_1$, we conclude that if λ is not an eigenvalue of J_e, then λ must satisfy

$$1 - p_{\pm}(\lambda)\boldsymbol{e}_1^T\left(J_e - \lambda I\right)^{-1}\boldsymbol{e}_1 = 0\,. \tag{2.12}$$

To simplify (2.12), we write $\left(J_e - \lambda I\right)^{-1}$ in terms of the cofactor matrix M as

$$\left(J_e - \lambda I\right)^{-1} = \frac{1}{\det(J_e - \lambda I)}M^T\,,$$

where the entries M_{ij} of M are the cofactors of the element $a_{i,j}$ of the matrix $J_e - \lambda I$. Since $\boldsymbol{e}_1^T\left(J_e - \lambda I\right)^{-1}\boldsymbol{e}_1 = M_{11}/\det\left(J_e - \lambda I\right)$, we obtain that (2.12) reduces to the following more explicit transcendental equation for λ:

$$1 - p_{\pm}(\lambda)\frac{M_{11}(\lambda)}{\det\left(J_e - \lambda I\right)} = 0\,, \qquad \text{where} \qquad M_{11}(\lambda) \equiv \det\begin{pmatrix} \left.\frac{\partial \mathcal{F}_2}{\partial u_2}\right|_{\boldsymbol{u}=\boldsymbol{u}_e} - \lambda, & \cdots, & \left.\frac{\partial \mathcal{F}_2}{\partial u_n}\right|_{\boldsymbol{u}=\boldsymbol{u}_e} \\ \cdots, & \cdots, & \cdots \\ \left.\frac{\partial \mathcal{F}_n}{\partial u_2}\right|_{\boldsymbol{u}=\boldsymbol{u}_e}, & \cdots, & \left.\frac{\partial \mathcal{F}_n}{\partial u_n}\right|_{\boldsymbol{u}=\boldsymbol{u}_e} - \lambda \end{pmatrix}. \tag{2.13}$$

Here $\mathcal{F}_2, \ldots, \mathcal{F}_n$ denote the components of the vector $\boldsymbol{\mathcal{F}} \equiv (\mathcal{F}_1, \ldots, \mathcal{F}_n)^T$ characterizing the membrane kinetics.

For the special case of a two-component membrane dynamics of the form $\boldsymbol{\mathcal{F}} = (f, g)^T$, with $f = f(u_1, u_2)$ and $g = g(u_1, u_2)$, (2.13) reduces to

$$1 - \frac{(g_{u_2} - \lambda)}{\det\left(J_e - \lambda I\right)}p_{\pm}(\lambda) = 0\,, \qquad J_e \equiv \begin{pmatrix} \left.\frac{\partial f}{\partial u_1}\right|_{\boldsymbol{u}=\boldsymbol{u}_e}, & \left.\frac{\partial f}{\partial u_2}\right|_{\boldsymbol{u}=\boldsymbol{u}_e} \\ \left.\frac{\partial g}{\partial u_1}\right|_{\boldsymbol{u}=\boldsymbol{u}_e}, & \left.\frac{\partial g}{\partial u_2}\right|_{\boldsymbol{u}=\boldsymbol{u}_e} \end{pmatrix}, \tag{2.14}$$

where $p_{\pm}(\lambda)$ are defined in (2.6) and (2.8). An example of this case is considered below in §5.

3 One-Component Membrane Dynamics

In this section we study the stability of steady-state solutions when the membrane dynamics consists of only a single component. For this case, it is convenient to label $u_1 = u$ and to define $F\left(C(0,t),u\right)$ by

$$F\left(C(0,t),u\right) \equiv \mathcal{F}(u) + \beta \mathcal{P}\left(C(0,t),u\right) . \tag{3.1}$$

The symmetric steady-state solution $C_e(x)$ is given by (2.2 *a*), where C_e^0 and u_e satisfy the nonlinear algebraic system

$$-C_e^0 \tanh(\omega_0 L) = \omega_0 G\left(C_e^0, u_{1e}\right) , \qquad F\left(C_e^0, u_e\right) = 0 , \qquad \text{where} \qquad \omega_0 \equiv 1/\sqrt{D} . \tag{3.2}$$

In terms of F defined in (3.1), the spectral problem characterizing the stability properties of this steady-state solution for either the synchronous or asynchronous mode is

$$D\Omega_\lambda \tanh(\Omega_\lambda L) = -G_c^e + \frac{F_c^e G_u^e}{F_u^e - \lambda} , \quad (\text{sync}) , \qquad D\Omega_\lambda \coth(\Omega_\lambda L) = -G_c^e + \frac{F_c^e G_u^e}{F_u^e - \lambda} , \quad (\text{async}) , \tag{3.3}$$

where $\Omega_\lambda \equiv \sqrt{(1+\tau\lambda)/D}$ is the principal branch of the square root. We will first derive theoretical results for the roots of (3.3) for the infinite-line problem where $L \to \infty$.

3.1 Theoretical Results for a Hopf Bifurcation: The Infinite-Line Problem

For the infinite-line problem where $L \to \infty$, (3.3) reduces to the limiting spectral problem of finding the roots of $\mathcal{G}(\lambda) = 0$ in $\mathrm{Re}(\lambda) \geq 0$, where

$$\mathcal{G}(\lambda) \equiv \sqrt{1+\tau\lambda} - g(\lambda) , \qquad \text{and} \qquad g(\lambda) \equiv \frac{c + a\lambda}{b + \lambda} . \tag{3.4 a}$$

Here the constants a, b, and c, are defined by

$$a \equiv -\frac{G_c^e}{\sqrt{D}} , \qquad b \equiv -F_u^e , \qquad c \equiv \frac{1}{\sqrt{D}} \left[G_c^e F_u^e - G_u^e F_c^e\right] . \tag{3.4 b}$$

Our goal is to characterize any roots of $\mathcal{G}(\lambda) = 0$ in $\mathrm{Re}(\lambda) > 0$ as the coefficients a, b, and c, are varied, and in particular to detect any Hopf bifurcation points. In (3.4), b represents the dependence of the local kinetics on the membrane-bound species. If $b > 0$, this term indicates a self-inhibiting effect, whereas if $b < 0$ the membrane-bound species is self-activating. The sign of G_c^e indicates the feedback from the environment to its own secretion. If G_c^e is positive (negative) it represents negative (positive) feedback. We remark that the spectral problem (3.4) has the same form, but with different possibilities regarding the signs of the coefficients, as the spectral problem studied in [**23**] characterizing the stability of a pulse solution for a singularly perturbed reaction-diffusion on the infinite line.

We first use a winding number argument to count the number N of roots of $\mathcal{G}(\lambda) = 0$ in $\mathrm{Re}(\lambda) \geq 0$ in terms of the behavior of $\mathcal{G}(\lambda)$ on the imaginary axis of the λ-plane. If $N = 0$, the symmetric steady-state solution is linearly stable, whereas if $N > 0$ this solution is unstable.

Lemma 3.1 *Let N be the number of zeroes of $\mathcal{G}(\lambda) = 0$ in $Re(\lambda) > 0$, where $\mathcal{G}(\lambda)$ is defined in (3.4). Assume that there are no such zeroes on the imaginary axis. Then,*

$$N = \frac{1}{4} + \frac{1}{\pi} \left[\arg\, \mathcal{G}\right]\Big|_{\Gamma_{I_+}} + P , \tag{3.5}$$

where $P = 0$ if $b > 0$ and $P = 1$ if $b < 0$. Here $\left[\arg\, \mathcal{G}\right]\big|_{\Gamma_{I_+}}$ denotes the change in the argument of $\mathcal{G}(\lambda)$ along the semi-infinite imaginary axis $\lambda = i\omega$ with $0 < \omega < \infty$, traversed in the downwards direction.

Proof: We take the counterclockwise contour consisting of the imaginary axis $-iR \leq \mathrm{Im}\lambda \leq iR$, decomposed as $\Gamma_{I_+} \cup \Gamma_{I_-}$,

where $\Gamma_{I_+} = i\omega$ and $\Gamma_{I_-} = -i\omega$ with $0 < \omega < R$, together with the semi-circle Γ_R, given by $|\lambda| = R > 0$ with $|\arg\lambda| \le \frac{\pi}{2}$. We use the argument principle of complex analysis to obtain

$$\lim_{R\to\infty} [\arg\,\mathcal{G}]\,\big|_C = 2\pi(N-P)\,, \qquad C \equiv \Gamma_R \cup \Gamma_{I_+} \cup \Gamma_{I_-}\,, \tag{3.6}$$

where $[\arg\mathcal{G}]\,\big|_C$ denotes the change in the argument of $\mathcal{G}$ over the contour C traversed in the counter-clockwise direction, and P is the number of poles of $\mathcal{G}$ inside C. Clearly $P = 1$ if $b < 0$ and $P = 0$ if $b > 0$. We calculate $\mathcal{G}(\lambda) \sim \sqrt{\tau R}e^{i\theta/2}$ on Γ_R as $R \to \infty$, where $\theta = \arg\lambda$, so that $\lim_{R\to\infty}[\arg\,\mathcal{G}]_{\Gamma_R} = \pi/2$. Moreover, since $\mathcal{G}(\overline{\lambda}) = \overline{\mathcal{G}(\lambda)}$, we get that $[\arg\,\mathcal{G}]_{\Gamma_{I_+}} = [\arg\,\mathcal{G}]_{\Gamma_{I_-}}$. In this way, we solve for N in (3.6) to obtain (3.5). ■

Next, we set $\lambda = i\omega$ in (3.4 *a*) to calculate $[\arg\,\mathcal{G}]\,\big|_{\Gamma_{I_+}}$ and detect any Hopf bifurcation points. Since we have specified the principal branch of the square root in (3.4 *a*), we must have that $\mathrm{Re}(\sqrt{1+\tau\lambda}) > 0$. Therefore, if we square both sides of the expression for $\mathcal{G} = 0$ in (3.4 *a*) and solve for τ, we may obtain spurious roots. We must then ensure that $\mathrm{Re}(g) > 0$ at any such root. Upon setting $\lambda = i\omega$ in (3.4 *a*) and squaring both sides, we obtain that $\tau = i\big(1 - [g(i\omega)]^2\big)/\omega$. Upon taking the real and imaginary parts of this expression we conclude that

$$\tau = \frac{1}{\omega}\mathrm{Im}\left([g(i\omega)]^2\right) = \frac{2}{\omega}g_R(\omega)g_I(\omega) = \frac{2(cb+a\omega^2)}{\left(b^2+\omega^2\right)^2}(ab-c)\,. \tag{3.7 a}$$

Here $\omega > 0$ is a root of

$$\mathrm{Re}\left([g(i\omega)]^2\right) = 1\,, \tag{3.7 b}$$

for which $g_R(\omega) > 0$ and $g_I(\omega) > 0$ to ensure that $\mathrm{Re}(\sqrt{1+i\tau\omega}) > 0$ and $\tau > 0$, respectively. In (3.7 *a*), $g(i\omega)$ has been decomposed into real and imaginary parts as $g(i\omega) = g_R(\omega) + ig_I(\omega)$, where

$$g_R(\omega) = \frac{bc+a\omega^2}{b^2+\omega^2}\,, \qquad g_I(\omega) = \frac{\omega(ab-c)}{b^2+\omega^2}\,. \tag{3.7 c}$$

In addition, if we separate $\sqrt{1+i\tau\omega}$ into real and imaginary parts, we readily derive that

$$\mathrm{Re}\left(\sqrt{1+i\tau\omega}\right) = \frac{1}{\sqrt{2}}\left[\sqrt{1+\tau^2\omega^2}+1\right]^{1/2}\,, \qquad \mathrm{Im}\left(\sqrt{1+i\tau\omega}\right) = \frac{1}{\sqrt{2}}\left[\sqrt{1+\tau^2\omega^2}-1\right]^{1/2}\,. \tag{3.8}$$

We now apply the winding number criterion of Lemma 3.1 together with (3.7) to determine the location of the roots of $\mathcal{G}(\lambda) = 0$ for various ranges of a, b, and c, as the parameter τ is varied.

Proposition 3.1 *Suppose that $cb < 0$ and that $a \le 0$. Then, no Hopf bifurcations are possible as $\tau > 0$ is varied. Moreover, if $b > 0$ we have $N = 0$, so that the symmetric steady-state solution is linearly stable for all $\tau > 0$. Alternatively, when $b < 0$ we have $N = 1$, and so the symmetric steady-state solution is unstable for all $\tau > 0$.*

Proof: We note that $g(\lambda)$, defined in (3.4 *a*), is a bilinear form and is real-valued when λ is real. It does not have a pole at $\lambda = 0$ since $b \neq 0$. Therefore, it follows that the imaginary axis $\lambda = i\omega$ must map to a disk $\mathcal{B}$ centered on the real axis in the (g_R, g_I) plane. When $cb < 0$ and $a \le 0$, it follows from (3.7 *c*) that $g_R < 0$, and so this disk lies in the left half-plane $\mathrm{Re}(g) < 0$. When $b > 0$, we have that $g(\lambda)$ is analytic in $\mathrm{Re}(\lambda) > 0$, and so the region $\mathrm{Re}(\lambda) > 0$ must map to inside the disk $\mathcal{B}$. As such, since $\mathrm{Re}\left(\sqrt{1+\tau\lambda}\right) > 0$, it follows that there are no roots to $\mathcal{G}(\lambda) = 0$ in $\mathrm{Re}(\lambda) > 0$, and so $N = 0$.

For the case $b < 0$, we use the winding number criterion (3.5). Since $cb < 0$ and $a \le 0$, we have $g_R(\omega) < 0$, so that $\mathrm{Re}\,[\mathcal{G}(i\omega)] = \mathrm{Re}\left[\sqrt{1+i\tau\omega} - g(i\omega)\right] > 0$. We have $\arg\mathcal{G}(i\omega) \to \pi/4$ as $\omega \to +\infty$ and $\mathcal{G}(0) > 0$, so that $\arg\mathcal{G}(0) = 0$. This yields that $[\arg\,\mathcal{G}]\,\big|_{\Gamma_{I_+}} = -\pi/4$. In addition, since $P = 1$ in (3.5), we obtain that $N = 1$ for all $\tau > 0$. ■

Next, we establish the following additional result that characterizes N, independent of the value of $\tau > 0$.

Proposition 3.2 *When $c > ab$, there are no Hopf bifurcation points for any $\tau > 0$. If in addition, we have*

$$\begin{aligned}
&(I) \quad b > 0\,, \ \textit{and}\ c/b < 1\,, \quad \textit{then,}\ N = 0 \ \forall \tau > 0\,,\\
&(II) \quad b < 0\,, \ \textit{and}\ c/b < 1\,, \quad \textit{then,}\ N = 1 \ \forall \tau > 0\,,\\
&(III) \quad b > 0\,, \ \textit{and}\ c/b > 1\,, \quad \textit{then,}\ N = 1 \ \forall \tau > 0\,,\\
&(IV) \quad b < 0\,, \ \textit{and}\ c/b > 1\,, \quad \textit{then,}\ N = 2 \ \forall \tau > 0\,.
\end{aligned} \tag{3.9}$$

Proof: We first observe from (3.8) and (3.7 *c*) that $\mathrm{Im}(\mathcal{G}(i\omega)) > 0$ for all $\tau > 0$ when $c > ab$. Therefore, there can be no Hopf bifurcations as τ is increased. To establish (I) of (3.9) we use $\mathcal{G}(0) > 0$, since $c/b < 1$, $\arg \mathcal{G}(i\omega) \to \pi/4$ as $\omega \to +\infty$, and $\mathrm{Im}(\mathcal{G}(i\omega)) > 0$ to conclude that $[\arg\, \mathcal{G}]\,\big|_{\Gamma_{I_+}} = -\pi/4$. Then, since $b > 0$ we have $P = 0$, and (3.5) yields $N = 0$. The proof of (II) of (3.9) is identical except that we have $P = 1$ in (3.5) since $b < 0$, so that $N = 1$. This unstable eigenvalue is located on the positive real axis on the interval $-b < \lambda < \infty$. To prove (III) we note that $\mathcal{G}(0) < 0$ since $c/b > 1$, and $P = 0$ since $b > 0$. This yields $[\arg\, \mathcal{G}]\,\big|_{\Gamma_{I_+}} = 3\pi/4$, and $N = 1$ from (3.5). This root is located on the positive real axis. Finally, to prove (IV) we use $\mathcal{G}(0) < 0$ and $b < 0$ to calculate $[\arg\, \mathcal{G}]\,\big|_{\Gamma_{I_+}} = 3\pi/4$ and $P = 1$. This yields $N = 2$ from (3.5). A simple plot of $\sqrt{1+\tau\lambda}$ and $g(\lambda)$ on the positive real axis for this case shows that there is a real root in $0 < \lambda < -b$ and in $-b < \lambda < \infty$ for any $\tau > 0$. ■

Next, we consider the range $ab > c$ and $bc > 0$ for which Hopf bifurcations in τ can be established for certain subranges of a, b, and c. To analyze this possibility, we substitute $g(i\omega)$ into (3.7 *b*), to obtain that ω must satisfy

$$\left(a\omega^2 + bc\right)^2 - \omega^2(ab - c)^2 = \left(b^2 + \omega^2\right)^2\,,$$

in the region $bc + a\omega^2 > 0$. Upon defining $\xi = \omega^2$, it follows for $|a| \neq 1$ that we must find a root of the quadratic $Q(\xi) = 0$ with $\xi \in \mathcal{S}$, where

$$Q(\xi) \equiv \xi^2 - a_0\xi + a_1 = (\xi - a_0/2)^2 + a_1 - a_0^2/4\,, \qquad \mathcal{S} \equiv \{\xi \mid \xi > 0 \text{ and } a\xi > -cb\}\,. \tag{3.10 a}$$

We refer to $\mathcal{S}$ as the admissible set. Here a_0 and a_1 are defined by

$$a_0 = \frac{1}{a^2-1}\left[(ab-c)^2 + 2b(b-ac)\right]\,, \qquad a_1 = \frac{b^2}{1-a^2}\left(b^2 - c^2\right)\,. \tag{3.10 b}$$

For the special case where $a = \pm 1$, we have

$$\xi = b^2\left(\frac{c/b - 1}{c/b + 3}\right)\,, \quad \text{if } a = -1\,; \qquad \xi = -b^2\left(\frac{c/b + 1}{3 - c/b}\right)\,, \quad \text{if } a = 1\,. \tag{3.10 c}$$

Our first result shows shows that there are certain subranges of the regime $ab > c$ and $bc > 0$ for which we again have that no Hopf bifurcations can occur for any $\tau > 0$.

Proposition 3.3 *Suppose that $b < 0$, $0 < c/b < 1$, and $c/b > a$. Then, $N = 1$ for all $\tau > 0$.*

Proof: We first establish, for any $\tau > 0$, that $\mathrm{Re}(\mathcal{G}(i\omega)) > 0$ when $\omega > 0$. We observe from (3.8) that $\mathrm{Re}(\sqrt{1 + i\tau\omega})$ is a monotone increasing function of ω, while $g_R(\omega)$, defined in (3.7 *c*), is a monotone decreasing function of ω when $c/b > a$. This implies that $\mathrm{Re}(\mathcal{G}(i\omega))$ is monotone increasing in ω when $c/b > a$. Since $\mathrm{Re}(\mathcal{G}(0)) = 1 - c/b > 0$ when $c/b < 1$, we conclude that $\mathrm{Re}(\mathcal{G}(i\omega)) > 0$ for $\omega > 0$. Then, since $\mathrm{Re}(\mathcal{G}(i\omega)) \to +\infty$ as $\omega \to +\infty$, we obtain $[\arg\, \mathcal{G}]\,\big|_{\Gamma_{I_+}} = -\pi/4$. Using this result in (3.5), together with $P = 1$ since $b < 0$, we get that $N = 1$ for all $\tau > 0$. ■

We now use Lemma 3.1 and (3.10) to identify a parameter regime in the range $ab > c$ with $bc > 0$ where there is a unique Hopf bifurcation value for τ:

Proposition 3.4 *Suppose that $b < 0$, $c/b > 1$ and $a < 1$. Then, we have either $N = 0$ or $N = 2$ for all $\tau > 0$. Moreover, $N = 0$ for $0 < \tau \ll 1$ and $N = 2$ for $\tau \gg 1$. For $a \neq -1$, there is a unique Hopf bifurcation at $\tau = \tau_H > 0$ given by*

$$\tau_H = \frac{2(cb + a\omega_H^2)}{\left(b^2 + \omega_H^2\right)^2}(ab - c)\,, \qquad \omega_H = \sqrt{\frac{a_0}{2} + \zeta\sqrt{\frac{a_0^2}{4} - a_1}}\,, \tag{3.11 a}$$

where $\zeta = +1$ if $|a| < 1$ and $\zeta = -1$ if $a < -1$. Here a_0 and a_1 are defined in (3.10 b). When $a = -1$, we have

$$\tau_H = -\frac{2(cb - \omega_H^2)}{\left(b^2 + \omega_H^2\right)^2}(b + c)\,, \qquad \omega_H = |b|\sqrt{\frac{c/b - 1}{c/b + 3}}\,. \tag{3.11 b}$$

Proof: We first establish that, for any $\tau > 0$, there is a unique root $\omega^\star$ to $\mathrm{Re}(\mathcal{G}(i\omega)) = 0$ in $\omega > 0$. To prove this we follow the proof of Proposition 3.3 to obtain that $\mathrm{Re}(\mathcal{G}(i\omega))$ is a monotone increasing function of ω when $c/b > a$. Moreover, since $\mathrm{Re}(\mathcal{G}(0)) = 1 - c/b < 0$, as a result of $c/b > 1$, and $\mathrm{Re}(\mathcal{G}(i\omega)) \to +\infty$ as $\omega \to +\infty$, we conclude that there is a a unique root $\omega^\star$ to $\mathrm{Re}(\mathcal{G}(i\omega)) = 0$ in the region $\omega > 0$. The uniqueness of the root to $\mathrm{Re}(\mathcal{G}(i\omega)) = 0$, together with the facts that $\mathcal{G}(0) = 1 - c/b < 0$ and $\arg\mathcal{G}(i\omega) \to \pi/4$ as $\omega \to +\infty$, establishes that either $[\arg\mathcal{G}]\big|_{\Gamma_{I_+}} = 3\pi/4$ or $[\arg\mathcal{G}]\big|_{\Gamma_{I_+}} = -5\pi/4$ depending on whether $\mathrm{Im}(\mathcal{G}(i\omega^\star)) > 0$ or $\mathrm{Im}(\mathcal{G}(i\omega^\star)) < 0$, respectively. Therefore, since $P = 1$, owing to the fact that $b < 0$, we conclude from (3.5) that either $N = 0$ or $N = 2$ for any $\tau > 0$.

To determine N when either $0 < \tau \ll 1$ or when $\tau \gg 1$, we examine the behavior of the unique root $\omega^\star$ to $\mathrm{Re}(\mathcal{G}(i\omega)) = 0$ for these limiting ranges of τ. For $\tau \gg 1$, we readily obtain that $\omega^\star = \mathcal{O}(1/\tau)$, so that $\mathrm{Im}(\mathcal{G}(i\omega^\star)) > 0$ from estimating $\mathrm{Im}(\sqrt{1 + i\tau\omega})$ and $g_I(\omega)$ in (3.8) and (3.7 c). Thus, $N = 2$ for $\tau \gg 1$. Alternatively, if $0 < \tau \ll 1$, we readily obtain that $\omega^\star = \mathcal{O}(1)$, and that $\mathrm{Im}(\mathcal{G}(i\omega^\star)) \sim -g_I(\omega^\star) + \mathcal{O}(\tau^2) < 0$. Therefore, $N = 0$ when $0 < \tau \ll 1$. By continuity with respect to τ it follows that there is a Hopf bifurcation at some $\tau > 0$.

To establish that the Hopf bifurcation value for τ is unique and to derive a formula for it, we now analyze the roots of $Q(\xi) = 0$ for $\xi \in \mathcal{S}$, where $Q(\xi)$ and the admissible set $\mathcal{S}$ are defined in (3.10). In our analysis, we must separately consider four ranges of a: (i) $0 \le a < 1$, (ii) $-1 < a < 0$, (iii) $a = -1$, and (iv) $a < -1$.

For (i) where $0 \le a < 1$, the admissible set $\mathcal{S}$ reduces to $\xi > 0$ since $cb > 0$. Moreover, we have $Q(0) = a_1 < 0$ since $c/b > 1$ and $Q \to +\infty$ as $\xi \to +\infty$. Since $Q(\xi)$ is a quadratic, it follows that there is a unique root to $Q(\xi) = 0$ in $\xi > 0$, with the other (inadmissible) root to $Q(\xi) = 0$ satisfying $\xi < 0$. By using (3.10 a) to calculate the largest root of $Q(\xi) = 0$, and recalling (3.7 a), we obtain (3.11 a).

The proof of (ii) for the range $-1 < a < 0$ is similar, but for this case the admissible set $\mathcal{S}$ is the finite interval $0 < \xi < -cb/a$. Since $Q(0) = a_1 < 0$ and Q is a quadratic, to prove that there is a unique root to $Q(\xi) = 0$ on this interval it suffices to show that $Q\left(-cb/a\right) > 0$. A straightforward calculation using the expressions for a_0 and a_1 in (3.10 b) yields, upon re-arranging terms in the resulting expression, that

$$\begin{aligned} Q\left(-cb/a\right) &= \frac{c^2b^2}{a^2} - \frac{cb}{a(1-a^2)}\left[(ab-c)^2 + 2b(b-ac)\right] + \frac{b^2(b^2-c^2)}{1-a^2}\,, \\ &= \frac{c^2b^2}{a^2} - \frac{cb}{a(1-a^2)}(ab-c)^2 + \frac{b^2}{1-a^2}\left[(b-c)^2 + 2cb\left(1 - \frac{1}{a}\right)\right]\,. \end{aligned}$$

Since $cb > 0$ and $-1 < a < 0$ all three terms in this last expression for $Q\,(-cb/a)$ are positive. Thus, there is a unique root to $Q(\xi) = 0$ in $0 < \xi < -cb/a$, which is given explicitly by (3.11 *a*).

When $a = -1$, the admissible set $\mathcal{S}$ is the interval $0 < \xi < cb$. It is then readily verified that the explicit formula for ξ given in (3.10 *c*) when $a = -1$ lies in this interval. In this way, we obtain (3.11 *b*).

Finally, we consider the range (iv) where $a < -1$, where the admissible set is $0 < \xi < -cb/a$. Since $c/b > 1$ and $a < -1$ we have from (3.10 *b*) that $a_0 > 0$ and $Q(0) = a_1 > 0$. Thus the minimum value of $Q(\xi)$ is at some point $\xi = \xi_m > 0$. To prove that there is a unique root to $Q(\xi) = 0$ on $0 < \xi < -cb/a$ we need only prove that $Q\,(-cb/a) < 0$. By re-arranging the terms in the expression for $Q\,(-cb/a)$ we obtain, after some algebra, that

$$Q\,(-cb/a) = -\frac{cb^3}{a^2(a^2-1)}\left[\frac{c}{b}(1+a^2) - a\left(\frac{c^2}{b^2}+a^2\right)\right] - \frac{b^2}{a^2-1}\left[(b-c)^2 + 2cb\frac{(a-1)}{a}\right].$$

Since $cb > 0$ and $a < -1$, we have that the expressions inside each of the two square brackets are positive, while the terms multiplying the square brackets are negative. This establishes that $Q\,(-cb/a) < 0$ and the existence of a unique root to $Q(\xi) = 0$ in $0 < \xi < -cb/a$. By taking the smallest root of $Q(\xi) = 0$ on $\xi > 0$ we get (3.11 *a*). ■

Our next result is for the case $b > 0$ on a subrange of where $ab - c > 0$.

Proposition 3.5 *The following results hold for the case $b > 0$: (I) Suppose that $c/b < a < 1$. Then, we have $N = 0$ for all $\tau > 0$. (II) Suppose that $c/b < 1 < a$. Then, there is a Hopf bifurcation at some $\tau = \tau_H > 0$. If $0 < \tau < \tau_H$, then $N = 2$, whereas if $\tau > \tau_H$, then $N = 0$. The Hopf bifurcation value $\tau_H > 0$ is given by*

$$\tau_H = \frac{2(cb + a\omega_H^2)}{\left(b^2+\omega_H^2\right)^2}(ab-c)\,, \qquad \omega_H = \sqrt{\frac{a_0}{2} + \sqrt{\frac{a_0^2}{4} - a_1}}\,, \tag{3.12}$$

where a_0 and a_1 are defined in (3.10 b).

Proof: We first prove (I). When $c/b < a < 1$, we have from (3.7 *c*) that $g_R(\omega)$ is monotone increasing with $c/b = g_R(0) < g_R(\omega) < g_R(\infty) = a < 1$. Since $\mathrm{Re}(\sqrt{1+i\omega\tau}) > 1$ for all $\tau > 0$, it follows that $\mathrm{Re}(\mathcal{G}(i\omega)) > 0$ on $0 \le \omega < \infty$, and consequently $[\arg\,\mathcal{G}]\big|_{\Gamma_{I_+}} = -\pi/4$. Then, since $P = 0$, owing to $b > 0$, (3.5) yields that $N = 0$ for all $\tau > 0$.

To prove (II) we consider the range $c \ge 0$ and $c < 0$ separately, and we first examine the roots to $Q(\xi) = 0$ for $\xi \in S$, as defined in (3.10). For the case $c \ge 0$, the admissible set is $\xi > 0$. Since the quadratic $Q(\xi)$ satisfies $Q(0) = a_1 < 0$ when $0 < c/b < 1 < a$, together with $Q(\xi) \to +\infty$ as $\xi \to \infty$, it follows that there is a unique root to $Q(\xi) = 0$ on $\xi > 0$. This yields the unique Hopf bifurcation value τ_H given in (3.12). Alternatively, suppose that $c < 0$. Then the admissible set is $\xi > -bc/a$. We calculate $Q\,(-bc/a)$ from (3.10), and after re-arranging the terms in the resulting expression, we obtain

$$\begin{aligned} Q\,(-cb/a) &= \frac{c^2b^2}{a^2} + \frac{cb}{a(a^2-1)}\left[(ab-c)^2 + 2b(b-ac)\right] + \frac{b^2(b^2-c^2)}{1-a^2}\,, \\ &= \frac{bc}{a}\frac{(ab-c)^2}{a^2-1} + \frac{b^2(b^2-c^2)}{1-a^2} + \frac{c^2b^2}{a^2(a^2-1)}\left[-a^2 - 1 + \frac{2ab}{c}\right]. \end{aligned}$$

Since each of the three terms in the last expression is negative when $c/b < 1 < a$, we have $Q\,(-bc/a) < 0$. It follows that there is a unique root to $Q(\xi) = 0$ on $-bc/a < \xi < \infty$, and consequently a unique Hopf bifurcation point.

Combining the results for $c \ge 0$ and $c < 0$, we conclude that there is a unique Hopf bifurcation point $\tau_H > 0$ when $c/b < 1 < a$ and $b > 0$. We now must prove the result that $N = 0$ for $\tau > \tau_H$ and $N = 2$ for $0 < \tau < \tau_H$. To establish this result, we need only prove than $N = 0$ for $\tau \gg 1$ and $N = 2$ for $0 < \tau \ll 1$. Then, by the uniqueness of τ_H, the continuity of λ with respect to τ, and the fact that $\lambda = 0$ cannot be eigenvalue, the result follows. For $\tau \gg 1$, we obtain

from the unboundedness of $\mathrm{Re}(\sqrt{1+i\tau\omega})$ as $\tau \to +\infty$ for $\omega > 0$ fixed that $\mathrm{Re}(\mathcal{G}(i\omega)) > 0$ on $0 \le \omega < \infty$ when $\tau \gg 1$. Therefore, since $[\arg \mathcal{G}]\big|_{\Gamma_{I_+}} = -\pi/4$ and $P = 0$, owing to $b > 0$, (3.5) yields that $N = 0$ for $\tau \gg 1$. Next, since $a > 1$, we readily observe that there are exactly two roots $\omega_\pm$ with $0 < \omega_- < \omega_+$ to $\mathrm{Re}(\mathcal{G}(i\omega)) = 0$ on $0 < \omega < \infty$, with the property that $\omega_- = \mathcal{O}(1)$ and $\omega_+ = \mathcal{O}(\tau^{-1}) \gg 1$ when $0 < \tau \ll 1$. We readily estimate that $\mathrm{Im}\,(\mathcal{G}(i\omega_+)) > 0$ and $\mathrm{Im}\,(\mathcal{G}(i\omega_-)) < 0$ when $\tau \ll 1$. Therefore, since $\arg \mathcal{G}(i\omega) \to \pi/4$ as $\omega \to +\infty$ and $\arg \mathcal{G}(0) = 0$ since $c/b < 1$, we conclude that $[\arg \mathcal{G}]\big|_{\Gamma_{I_+}} = 7\pi/4$ when $0 < \tau \ll 1$. Finally, since $P = 0$, owing to $b > 0$, (3.5) yields $N = 2$ when $0 < \tau \ll 1$. ■

Our final result is for the range $1 < a < c/b$ with $b < 0$ where there can be either two Hopf bifurcation values of τ or none.

Proposition 3.6 *Suppose that $b < 0$ and $1 < a < c/b$. Then, if $c/b \le 3a + 2\sqrt{2}(a^2-1)^{1/2}$, we have $N = 2$ for all $\tau > 0$, and consquently no Hopf bifurcation points. Alternatively, if $c/b > 3a + 2\sqrt{2}(a^2-1)^{1/2}$, then there are two Hopf bifurcation values $\tau_{H\pm}$, with $\tau_{H-} > \tau_{H+}$, so that $N = 0$ for $\tau_{H+} < \tau < \tau_{H-}$ and $N = 2$ when either $0 < \tau < \tau_{H+}$ or $\tau > \tau_{H-}$.*

Proof: Since the proof of this result is similar to those of Propositions 3.4 and 3.5, we only briefly outline the derivation. First, since necessarily $c < 0$, the admissible set for $Q(\xi)$ in (3.10 *a*) is $\xi \ge 0$, and hence we focus on determining whether $Q(\xi) = 0$ has any positive real roots. For the range $1 < a < c/b$, we calculate $Q(0) = a_1 > 0$ from (3.10). As such it follows that there are either two real roots to $Q(\xi) = 0$ in $\xi > 0$, a real positive root of multiplicty two, or no real roots. From (3.10), there are two real roots only when $a_0 > 0$ and $a_0^2/4 - a_1 > 0$, where a_0 and a_1 are defined in (3.10 *b*).

Upon using (3.10 *b*) for a_0 and a_1, we can show after some lengthy but straightforward algebra that $a_0 > 0$ when $c/b > 2a + \sqrt{3a^2-2}$, and $a_0^2/4 - a_1 > 0$ when

$$\left(\frac{c}{b} - 3a\right)^2 + 8(1-a^2) > 0\,.$$

For any $a > 1$, the intersection of these two ranges of c/b is $c/b > 3a + 2\sqrt{2}(a^2-1)^{1/2}$. On this range, $Q(\xi) = 0$ has two positive real roots, and hence there are two Hopf bifurcation values of τ. For the range $1 < a < c/b < 3a + 2\sqrt{2}(a^2-1)^{1/2}$, then either $a_0 < 0$ or $a_0^2/4 - a_1 < 0$, and so $Q(\xi) = 0$ has no positive real roots.

The determination of N follows in a similar way as in the proof of Proposition 3.5. ■

3.2 A Finite Domain: Numerical Computations of the Winding Number

For finite domain length L, the synchronous and asychronous modes will, in general, have different instability thresholds. For finite L, we use (3.3) to conclude that we must find the roots of $\mathcal{G}(\lambda) = 0$, where we now re-define $\mathcal{G}(\lambda)$ as

$$\mathcal{G}(\lambda) \equiv D\Omega_\lambda h\,(\Omega_\lambda) + G_c^e - \frac{F_c^e G_u^e}{F_u^e - \lambda}\,, \qquad h(\Omega_\lambda) \equiv \begin{cases} \tanh\,(\Omega_\lambda L)\,, & (\textit{synchronous}) \\ \coth\,(\Omega_\lambda L)\,, & (\textit{asynchronous}) \end{cases}, \tag{3.13 a}$$

where $\Omega_\lambda = \sqrt{(1+\tau\lambda)/D}$. It is readily shown that (3.5) still holds, and so

$$N = \frac{1}{4} + \frac{1}{\pi}\,[\arg\,\mathcal{G}]\,\big|_{\Gamma_{I_+}} + P\,, \tag{3.13 b}$$

where $P = 0$ if $F_u^e < 0$ and $P = 1$ if $F_u^e > 0$. To determine N for a specific membrane-bulk system, numerical computations of $[\arg\,\mathcal{G}]\,\big|_{\Gamma_{I_+}}$ must be performed separately for both the synchronous and asynchronous modes. This is illustrated below in §4 for some specific membrane-bulk systems.

We remark that some of the results in §3.1 are still valid when L is finite. To see this, we write (3.13 *a*) in the form

$$\sqrt{1+\tau\lambda}\,\frac{h(\Omega_\lambda)}{h(\omega_0)} = g(\lambda)\,, \qquad g(\lambda) \equiv \frac{c_L + a_L\lambda}{b+\lambda}\,, \tag{3.14 a}$$

where $\omega_0 = D^{-1/2}$, and where we have defined a_L, b, and c_L, by

$$a_L \equiv -\frac{G_c^e}{\sqrt{D}h(\omega_0)}\,, \qquad b \equiv -F_u^e\,, \qquad c_L \equiv \frac{1}{\sqrt{D}h(\omega_0)}\left[G_c^eF_u^e - G_u^eF_c^e\right]\,. \tag{3.14 b}$$

We remark that as $L\to\infty$, (3.14) reduces to the eigenvalue problem (3.4 *a*) for the infinite-line problem studied in §3.1.

With this reformulation, the left-hand side of (3.14 *a*) has the same qualitative properties as $\sqrt{1+\tau\lambda}$ that were used in the proofs of some of the propositions in §3.1. In particular, Propositions 3.1–3.3 and part (I) of Proposition 3.5 still apply provided we replace a and c in these results by a_L and c_L. We do not pursue this extension any further here.

4 Examples of the Theory: One-Component Membrane Dynamics

In this section we consider some specific systems to both illustrate our stability theory and to show the existence of synchronous and asynchronous oscillatory instabilities induced by coupled membrane-bulk dynamics. Assuming a one-component membrane dynamics, we determine the stability of the steady-state solution by numerically computing the number N of eigenvalues of the linearization in $\mathrm{Re}(\lambda) > 0$ from either (3.5) for the infinite-line problem, or from (3.13) for the finite-domain problem. For some subranges of the parameters in these systems, the theoretical results of §3.1 for the infinite-line problem determines N without the need for any numerical winding number computation.

To confirm our stability results for the case of a one-component membrane dynamics we also computed symmetric steady-state solutions of (1.1) and bifurcations of this solution to periodic solutions by first spatially discretizing (1.1) with finite differences. Then, from this method of lines approach, together with the path continuation program AUTO with the interface provided by XPPAUT (cf. [**6**]), branches of steady-state and periodic solution branches were computed numerically. To confirm predictions of oscillatory dynamics, full time-dependent numerical solutions of the coupled PDE-ODE system (1.1) were computed using the method of lines.

4.1 A Class of Feedback Models

We first apply the theory of §3.1 to a class of membrane-bulk problems on the infinite line, corresponding to letting $L\to\infty$, of the form

$$\begin{aligned} &\tau C_t = DC_{xx} - C\,, \qquad t>0\,, \quad x>0\,; \qquad DC_x\big|_{x=0} = G(C(0,t),u)\,; \quad C\to 0 \quad \text{as} \quad x\to\infty\,, \\ &\frac{du}{dt} = F(C(0,t),u)\,, \qquad \text{where} \qquad F(C(0,t),u) \equiv \mathcal{F}(u) + \sigma G(C(0,t),u(t))\,, \end{aligned} \tag{4.1}$$

for some $\sigma > 0$. For this class, the flux on $x=0$ acts as a source term to the membrane dynamics. A special case of (4.1), which is considered below, is when the membrane-bulk coupling is linear and, for some $\kappa>0$, has the form

$$G(C(0,t),u) \equiv \kappa\left[C(0,t) - u\right]\,. \tag{4.2}$$

To apply the theory in §3.1 to (4.1) we first must calculate a, b, and c, from (3.4 *b*). We readily obtain that

$$b = -\mathcal{F}'(u_e) - \sigma G_u^e\,, \qquad a = -\frac{G_c^e}{\sqrt{D}}\,, \qquad c = \frac{1}{\sqrt{D}}G_c^e\mathcal{F}'(u_e)\,, \qquad ab - c = \frac{\sigma}{\sqrt{D}}G_u^eG_c^e\,, \tag{4.3}$$

where u_e is a steady-state value for u. The first result for (4.1) shows that a Hopf bifurcation is impossible with a linear membrane-bulk coupling mechanism.

Proposition 4.1 *Let C_e, u_e be the steady-state solution for (4.1) with the linear membrane-bulk coupling (4.2). Let N denote the number of unstable eigenvalues in $Re(\lambda) > 0$ for the linearization of (4.1) around this steady-state solution. Then, for any $\tau > 0$, we have $N = 0$ when $\mathcal{F}'(u_e) < \mathcal{F}_{Lth}$, and $N = 1$ when $\mathcal{F}'(u_e) > \mathcal{F}_{Lth}$, where $\mathcal{F}_{Lth} \equiv \sigma\kappa/\left[1 + \kappa/\sqrt{D}\right]$.*

Proof: Since with the coupling (4.2) we have $ab - c = -\kappa^2\sigma/\sqrt{D} < 0$, it follows by Proposition 3.2 that there are no Hopf bifurcations for any $\tau > 0$. To determine the stability threshold, we calculate $a = -\kappa/\sqrt{D} < 0$, $b = -\mathcal{F}'(u_e) + \sigma\kappa$, and $c = \kappa\mathcal{F}'(u_e)/\sqrt{D}$, and apply the results of Proposition 3.2. We separate our analysis into three ranges of $\mathcal{F}'(u_e)$. First suppose that $\mathcal{F}'(u_e) < 0$. Then, since $b > 0$, $c < 0$, and $a < 0$, we have by (I) of Proposition 3.2 that $N = 0$. Next, suppose that $0 < \mathcal{F}'(u_e) < \sigma\kappa$, so that $b > 0$ and $c > 0$. We calculate that $c/b > 1$ if $\mathcal{F}'(u_e) > \mathcal{F}_{\rm Lth}$, where $\mathcal{F}_{\rm Lth}$, which satisfies $0 < \mathcal{F}_{\rm Lth} < \sigma\kappa$, is defined above. Since $c/b > 1$, (III) of Proposition 3.2 proves that $N = 1$ for all $\tau > 0$. Alternatively, if $0 < \mathcal{F}'(u_e) < \mathcal{F}_{\rm Lth}$, then $c/b < 1$, and (I) of Proposition 3.2 proves that $N = 0$ for all $\tau > 0$. Finally, suppose that $\mathcal{F}'(u_e) > \sigma\kappa$. Then, $c > 0$, $b < 0$, so that $bc < 0$ and $a < 0$. We conclude from Proposition 3.1 that $N = 1$ for all $\tau > 0$. The proof is complete by combining these results on the three separate ranges of $\mathcal{F}'(u_e)$. ■

This result for the non-existence of oscillations for a linear membrane-bulk coupling mechanism holds only for the case of a single membrane-bound species. As shown in §5, when there are two species in the membrane, oscillatory dynamics can occur even with a linear membrane-bulk coupling mechanism. Our next result for (4.1) specifies a class of nonlinear coupling mechanisms $G(C(0,t),u)$ for which no Hopf bifurcations of the steady-state solution are possible.

Proposition 4.2 *When $G_c^e G_u^e < 0$, then the steady-state solution of (4.1) does not undergo a Hopf bifurcation for any $\tau > 0$. In particular, if $G_u^e < 0$ and $G_c^e > 0$, then for any $\tau > 0$ we have $N = 1$ when $\mathcal{F}'(u_e) > \mathcal{F}_{th}$, and $N = 0$ when $\mathcal{F}'(u_e) < \mathcal{F}_{th}$. Here $\mathcal{F}_{th} > 0$ is the threshold value*

$$\mathcal{F}_{th} \equiv -\frac{\sigma G_u^e}{1 + G_c^e/\sqrt{D}}\,. \tag{4.4}$$

Proof: From (4.3) we have $ab - c < 0$ when $G_c^e G_u^e < 0$. Proposition 3.2 proves that there are no Hopf bifurcations for any $\tau > 0$. The second part of the proof parallels that done for Proposition 4.2, and is left to the reader. ■

A similar analysis can be done for the case where $G_u^e > 0$ and $G_c^e < 0$. For this case, the steady-state solution is unstable when $G_c^e < -\sqrt{D}$ for all ranges of $\mathcal{F}'(u_e)$. When $G_c^e > -\sqrt{D}$, the steady-state is linearly stable only when $\mathcal{F}'(u_e) < -\sigma G_u^e/\left[1 + G_c^e/\sqrt{D}\right]$.

Our final result for (4.1) characterizes a class of nonlinear coupling mechanisms for which a Hopf bifurcation of the steady-state solution does occur for some value of τ.

Proposition 4.3 *Suppose that $G_c^e > 0$ and $G_u^e > 0$. Then, for the steady-state solution of (4.1), we have:*

$$\begin{aligned}
&(I) \quad \textit{If} \quad \mathcal{F}'(u_e) > \mathcal{F}_{th}\,, \quad \textit{then } N = 1 \ \forall \tau > 0\,,\\
&(II) \quad \textit{If} \quad -\sigma G_u^e < \mathcal{F}'(u_e) < \mathcal{F}_{th}\,, \quad \textit{then } N = 2 \textit{ for } \tau > \tau_H\,, \textit{ and } N = 0 \textit{ for } 0 < \tau < \tau_H\,,\\
&(III) \quad \textit{If} \quad \mathcal{F}'(u_e) < -\sigma G_u^e\,, \quad \textit{then } N = 0 \ \forall \tau > 0\,.
\end{aligned} \tag{4.5}$$

Here $\tau_H > 0$ is the unique Hopf bifurcation point, and $\mathcal{F}_{th} < 0$ is defined in (4.4).

Proof: Since $G_c^e > 0$, we have $a < 0$ from (4.3). To establish (III) we calculate from (4.3) that $b > 0$ and $c < 0$ when

$\mathcal{F}'(u_e) < -\sigma G_u^e$. From the first statement of Proposition 3.1, we conclude that $N = 0$. To establish (II), we observe that $b < 0$, $c < 0$, and $c/b > 1$ when $-\sigma G_u^e < \mathcal{F}'(u_e) < \mathcal{F}_{\rm th} < 0$. Proposition 3.4 then proves that there is a unique Hopf bifurcation value $\tau = \tau_H > 0$ on this range of $\mathcal{F}'(u_e)$, as given in (3.11). Finally, to establish (I), we observe that $b < 0$ and $c/b < 1$ when $\mathcal{F}'(u_e) > \mathcal{F}_{\rm th}$. For the range $c < 0$, where $\mathcal{F}_{\rm th} < \mathcal{F}'(u_e) < 0$, we have from Proposition 3.3 that $N = 1$. Finally, for the range $c > 0$, where $\mathcal{F}'(u_e) > 0$, Proposition 3.1 also yields that $N = 1$. ■

We now discuss the limiting behavior of τ_H and the corresponding Hopf bifurcation frequency ω_H, as given by (3.11), at the two edges of the interval for $\mathcal{F}'(u_e)$ in (II) of Proposition 4.3. First, we observe that as $\mathcal{F}'(u_e)$ approaches $-\sigma G_u^e$ from above, we have that $b \to 0^-$. Therefore, from (3.11) we have $a_1 \to 0$, and so at this lower edge of the interval we have $\omega_H \to 0^+$ and $\tau_H \to +\infty$. At the other end of the interval, where $\mathcal{F}'(u_e)$ approaches $\mathcal{F}_{\rm th}$ from below, we have that $c - b \to 0$, so that again $a_1 \to 0$ in (3.11). Therefore, from (3.11), we conclude at this upper edge of the interval that $\omega_H \to 0^+$. However, since $b = \mathcal{O}(1)$, we have from (3.11 *a*) that $\tau_H \to 2(1-a)/|b| = \mathcal{O}(1)$ at the upper edge.

4.2 A Phase Diagram for an Explicitly Solvable Model

Next, we consider a simple model where a phase diagram characterizing the possibility of Hopf bifurcations can be determined analytically for the infinite-line problem. For $\beta > 0$, $\gamma > 0$ and $\kappa > 0$, we consider

$$\begin{aligned} \tau C_t &= DC_{xx} - C\,, \qquad t > 0\,, \quad 0 < x < 2L\,, \\ DC_x\big|_{x=0} &= G(C(0,t),u) \equiv \kappa \frac{(C(0,t)-u)}{1+\beta\,(C(0,t)-u)^2}\,, \\ \frac{du}{dt} &= F(C(0,t),u) \equiv \gamma C(0,t) - u\,, \end{aligned} \tag{4.6}$$

with identical membrane dynamics at $x = 2L$. The symmetric steady-state solution for (4.6) is $C_e(x)$ given in (2.2 *a*), where $C_e^0 \equiv C_e(0)$ satisfies the cubic equation

$$(C_e^0)^3\beta(\gamma-1)^2\tanh(\omega_0 L) - C_e^0\left[\kappa\omega_0(\gamma-1) - \tanh(\omega_0 L)\right] = 0\,, \qquad \omega_0 \equiv \sqrt{1/D_0}\,. \tag{4.7}$$

In our analysis, we will focus on periodic solutions that bifurcate from the steady-state solution branch where C_e^0 is positive. From (4.7), the positive root is given explicitly by

$$C_e^0 = \sqrt{\frac{\kappa\omega_0(\gamma-1) - \tanh(\omega_0 L)}{\beta(\gamma-1)^2\tanh(\omega_0 L)}}\,, \qquad u_e = \gamma C_e^0\,, \qquad \text{when} \qquad \kappa\omega_0(\gamma-1) - \tanh(\omega_0 L) > 0\,. \tag{4.8}$$

We first consider the infinite-line problem where $L \to \infty$ and we set $D = 1$ for convenience. Then, (4.8) reduces to

$$C_e^0 = \sqrt{\frac{\kappa(\gamma-1) - 1}{\beta(\gamma-1)^2}}\,. \tag{4.9}$$

For this example, we calculate a, b, and c, in (3.4 *b*) as

$$a = -G_c^e = -\frac{1}{\kappa(\gamma-1)^2}\left[2 - \kappa(\gamma-1)\right]\,, \qquad b = 1\,, \qquad c = (\gamma-1)G_c^e\,, \qquad ab - c = -\gamma G_c^e\,. \tag{4.10}$$

We now apply the theory of §3.1 to obtain the phase-diagram Fig. 2 in the parameter space κ versus γ. Since $C_e^0 > 0$ only when $\gamma > 1$ and $\kappa > 1/(\gamma-1)$, the boundary between region I and II in Fig. 2 is $\kappa = 1/(\gamma-1)$. Next, we calculate that $ab - c < 0$ and $0 < c/b < 1$ when $(\gamma-1)^{-1} < \kappa < 2(\gamma-1)^{-1}$, which is labeled as region II in Fig. 2. Therefore, in this region, we conclude from condition (I) of Proposition 3.2 that the steady-state is stable for all $\tau > 0$. Next, we calculate from (4.10) that $c/b < a < 1$ when $2(\gamma-1)^{-1} < \kappa < 2(\gamma-1)^{-1}(2-\gamma)^{-1}$ and $\gamma > 1$, which is region III of Fig. 2. For this range, Proposition 3.5 proves that the steady-state solution is stable for all $\tau > 0$. Finally, region IV of Fig. 2 given

by $\kappa > 2(\gamma-1)^{-1}(2-\gamma)^{-1}$ for $1 < \gamma < 2$, is where $c/b < 1 < a$. At each point in this region, Proposition 3.5 proves that there is a Hopf bifurcation value $\tau = \tau_H > 0$, and that the steady-state solution is unstable if $0 < \tau < \tau_H$.

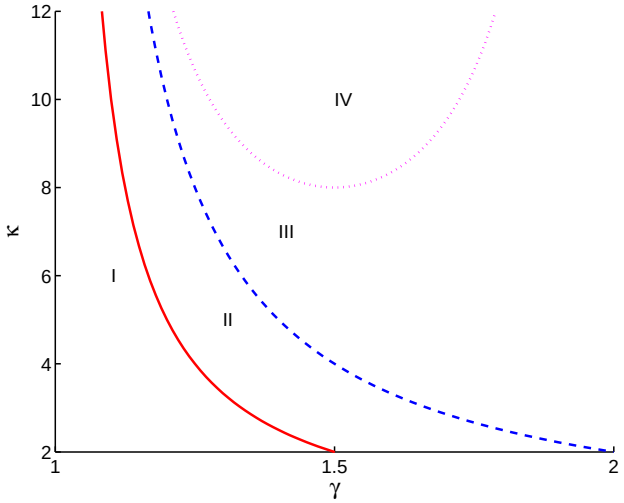

Figure 2. Phase diagram for (4.6) in the κ versus γ plane for the infinite-line problem when $D = 1$. In region I, $\kappa < (\gamma-1)^{-1}$ with $\gamma > 1$, and there is no steady-state solution. In region II, bounded by $(\gamma-1)^{-1} < \kappa < 2(\gamma-1)^{-1}$ for $\gamma > 1$, we have $ab - c < 0$ and $b > 0$, and the steady-state solution is linearly stable for all $\tau > 0$. In region III, bounded by $2(\gamma-1)^{-1} < \kappa < 2(\gamma-1)^{-1}(2-\gamma)^{-1}$ for $\gamma > 1$, we have $b > 0$ and $c/b < a < 1$, and so by the first statement in Proposition 3.5 there is no Hopf bifurcation and the steady-state solution is linearly stable for all $\tau > 0$. In region IV, bounded by $\kappa > 2(\gamma-1)^{-1}(2-\gamma)^{-1}$ for $1 < \gamma < 2$, we have $b > 0$ and $c/b < 1 < a$, and so by the second statement in Proposition 3.5 there is a Hopf bifurcation and the steady-state solution is unstable if $0 < \tau < \tau_H$ and is linearly stable if $\tau > \tau_H$, where $\tau_H > 0$ is given by (3.12).

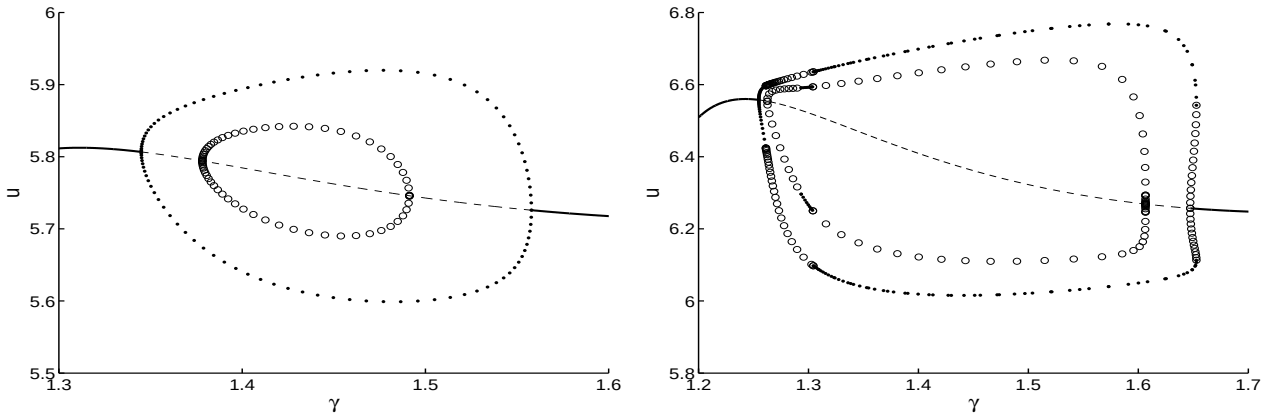

Figure 3. Two typical bifurcation diagrams for u versus γ for (4.6) on a finite domain with $L = 2$, $D = 1$, $\tau = 0.1$, and $\beta = 1$. Left panel: $\kappa = 9$. Right-panel: $\kappa = 10.5$. The solid and dashed lines denote linearly stable and unstable branches of steady-state solutions. The outer and inner closed loops correspond to branches of synchronous and asynchronous periodic solutions, respectively. The solid/open circles indicate linearly stable/unstable periodic solutions, respectively.

For the finite-domain problem with $L = 2$, and for two values of κ, in Fig. 3 we plot numerically computed bifurcation diagrams of u versus γ for both the steady-state and bifurcating periodic solution branches. For the corresponding infinite-line problem, this corresponds to taking a horizontal slice at fixed κ through the phase diagram of Fig. 2. The results in the left panel of Fig. 3 show that when $\kappa = 9$ the bifurcating branch of synchronous oscillations is linearly stable, while the

asynchronous branch is unstable. To confirm this prediction of a stable synchronous oscillation for $\kappa = 9$ and $\gamma = 1.45$, in Fig. 4 we plot the full numerical solution computed from the PDE-ODE system (4.6). Starting from the initial condition $C(x, 0) = 1$, together with $u_1(0) = 0.4$ and $u_2(0) = 0.5$ in the left and right membranes, respectively, this plot shows the eventual synchrony of the oscillations in the two membranes. In the right panel of Fig. 3, where $\kappa = 10.5$, we show that the synchronous mode is stable for a wide range of γ, but that there is a narrow parameter range in γ where both the synchronous and asynchronous modes are unstable. For the value $\gamma = 1.28$ within this dual-unstable zone, the full numerical solution of the PDE-ODE system (4.6), shown in Fig. 5 reveals a phase-locking phenomena in the oscillatory dynamics of the two membranes.

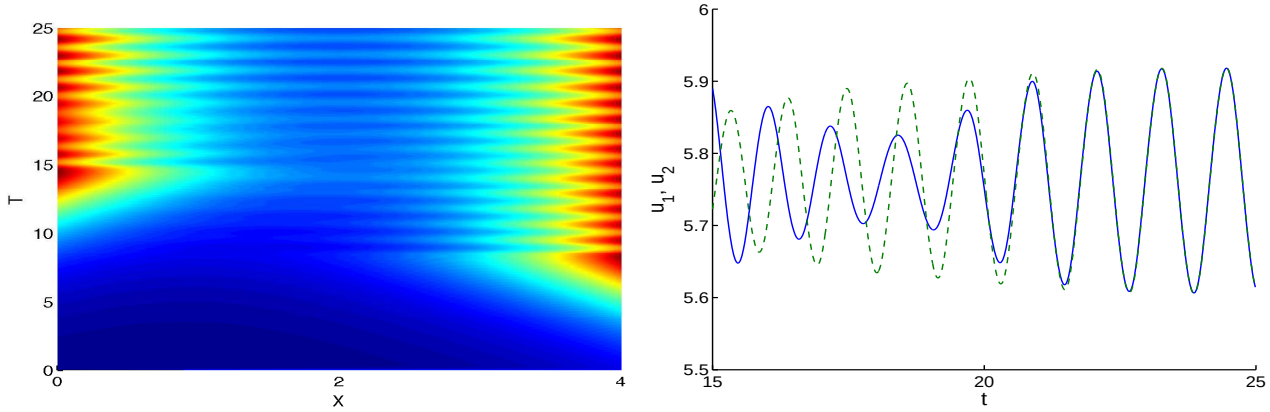

Figure 4. Full numerical solutions (left panel) of the PDE-ODE system for (4.6) for the finite-domain problem with $L = 2$, $D = 1$, $\tau = 0.1$, $\kappa = 9$, $\gamma = 1.45$, and $\beta = 1$. The initial condition is $C(x, 0) = 1$, with $u_1(0) = 0.4$ and $u_2(0) = 0.5$ in the left and right membranes. On the infinite line the parameter values are in region IV of Fig. 2. For this value of γ and κ we observe from the left panel of the global bifurcation diagram Fig. 3 that only the synchronous mode is stable. The full numerical solutions for u_1 and u_2 (right panel) confirm this prediction.

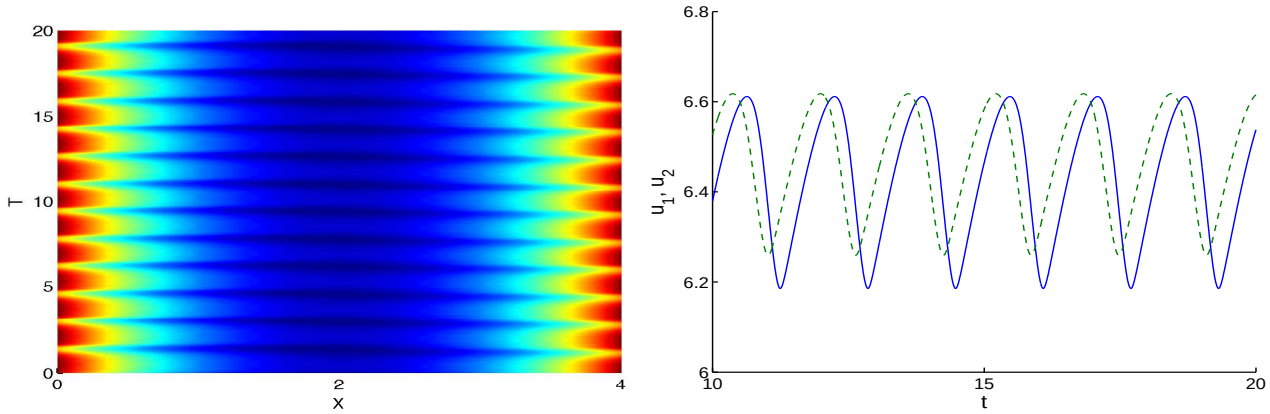

Figure 5. Full numerical solutions (left panel) of the PDE-ODE system for (4.6) for the finite-domain problem with $L = 2$, $D = 1$, $\tau = 0.1$, $\kappa = 10.5$, $\gamma = 1.28$, and $\beta = 1$. The initial condition is as given in Fig. 4. For this value of γ and κ we observe from the right panel of the global bifurcation diagram Fig. 3 that the synchronous and asynchronous periodic solutions are both linearly unstable. The full numerical solutions for u_1 and u_2 (right panel) reveal a phase-locking phenomenon.

4.3 Two Biologically-Inspired Models

Next, we consider two specific biologically-inspired models which undergo a Hopf bifurcation when parameters vary. The first example is a simplified version of the GnRH neuron model from [**13**, **19**, **7**]. In this context, the spatial variable $C(x,t)$ is the GnRH concentration in the bulk medium while u is the membrane concentration of the activated α-subunits of the G-protein G_i which is activated by the binding of GnRH to its receptor. As discussed in the Appendix, the functions describing the boundary flux and the membrane kinetics for this model are as follows:

$$G(C(0,t),u) = -\sigma\left[1+\beta\left(\frac{\iota+1+\zeta q}{\mu+1+\delta q}\right)^3\left(\eta+\frac{s}{\omega+u}\right)^3\right], \qquad F(C(0,t),u) = \epsilon\left(\frac{[C(0,t)]^2}{k_i^2+[C(0,t)]^2}-u\right), \tag{4.11 a}$$

where s and q, which depend on $C(0,t)$, are defined by

$$s \equiv \frac{[C(0,t)]^4}{k_s^4+[C(0,t)]^4}, \qquad q \equiv \frac{[C(0,t)]^2}{k_q^2+[C(0,t)]^2}. \tag{4.11 b}$$

The fixed parameters in this model, as discussed in [**13**, **19**, **7**], can be obtained from fitting experimental data.

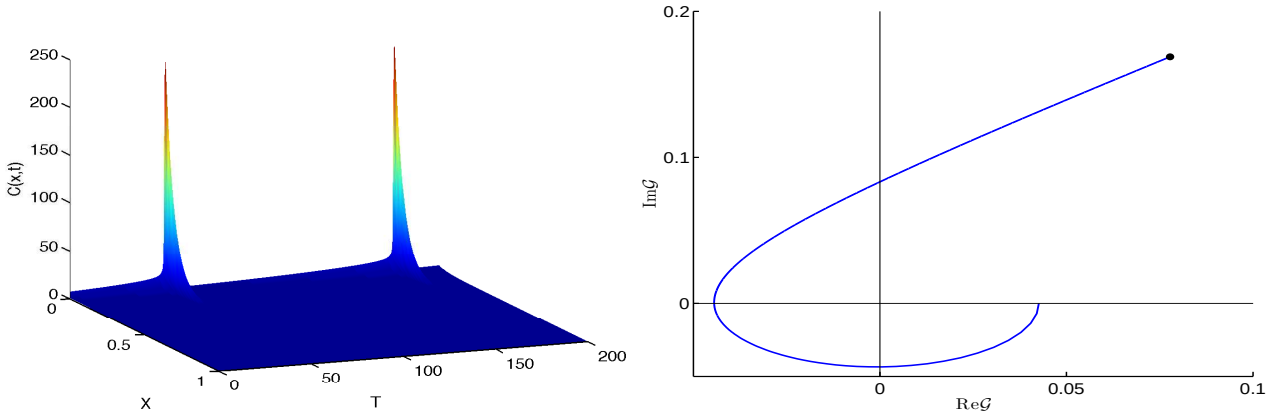

Figure 6. Left figure: Numerical results, showing oscillatory dynamics, for $C(x,t)$ in the GnRH model (4.11). The bulk diffusion parameters are $D = 0.003$, $\tau = 1$, and $L = 1$. The parameters in the membrane-bulk coupling and dynamics in (4.11) are $\sigma = 0.047$, $\beta = 5.256\times 10^{-14}$, $\iota = 764.7$, $\zeta = 3747.1$, $\mu = 0.012$, $\delta = 0.588$, $\eta = 0.410$, $\omega = 0.011$, $\epsilon = 0.0125$, $k_i = 464$, $k_s = 1$, and $k_q = 61$. Right figure: Plot of the imaginary part versus the real part of $\mathcal{G}(i\omega)$ when $\lambda = i\omega$ and ω decreases from 3 (black dot) to 0. This shows that the winding number $[\arg\,\mathcal{G}]\big|_{\Gamma_{I_+}}$ is $7\pi/4$, and so $N = 2$ from (3.13 a).

For the bulk diffusion process we let $D = 0.003$, $\tau = 1$, and $L = 1$. Since $L/\sqrt{D} \approx 18.3 \gg 1$, our analytical stability theory for the infinite-line problem will provide a good prediction for the stability properties associated with this finite-domain problem. By using the parameter values of [**13**], as written in the caption of Fig. 6, we calculate that

$$b = -F_u^e = \epsilon > 0\,, \qquad a = -G_c^e/\sqrt{D} > 0\,, \qquad F_c^e > 0\,, \qquad G_u^e > 0\,. \tag{4.12}$$

In the right panel of Fig. 6 we show a numerical computation of the winding number, which establishes that $[\arg\,\mathcal{G}]\big|_{\Gamma_{I_+}} = 7\pi/4$. Since $b > 0$, we conclude from (3.5) that $N = 2$. Our full numerical simulations of the PDE-ODE system in the left panel of Fig. 6, showing an oscillatory dynamics, is consistent with this theoretical prediction. In fact, for the parameter values in the caption of Fig. 6 we have $a = 1.8223$, $b = 0.0125$, and $c = 0.0028$. Since $b > 0$ and $c/b < 1 < a$, the second statement in Proposition 3.5 proves that there is a Hopf bifurcation value of τ for the corresponding infinite-line problem. We calculate $\tau_H \approx 113.5$ with frequency $\omega_H \approx 0.0169$, which indicates a rather large period of oscillation at onset.

Another specific biological system is a model of cell signaling in *Dictyostelium* (cf. [**9**]). In this context, the spatial

variable $C(x,t)$ is the concentration of the cAMP in the bulk region, while u is the total fraction of cAMP receptor in the active state on the two membranes (binding of cAMP to this state of the receptor elicits cAMP synthesis). As discussed in the Appendix, the boundary flux and nonlinear membrane dynamics for this system are described

$$G(C(0,t),u) = -\sigma^\star \frac{\alpha\left(\Lambda\theta + \frac{\epsilon u[C(0,t)]^2}{1+[C(0,t)]^2}\right)}{(1+\alpha\theta) + (\frac{\epsilon u[C(0,t)]^2}{1+[C(0,t)]^2})(1+\alpha)}\,, \qquad (4.13\,a)$$
$$F(C(0,t),u) = f_2(C(0,t)) - u[f_1(C(0,t)) + f_2(C(0,t))]\,,$$

where

$$f_1(C(0,t)) \equiv \frac{k_1 + k_2[C(0,t)]^2}{1+[C(0,t)]^2}\,, \qquad f_2(C(0,t)) \equiv \frac{k_1 L_1 + k_2 L_2 c_d^2[C(0,t)]^2}{1+c_d^2[C(0,t)]^2}\,. \qquad (4.13\,b)$$

The fixed parameters in this model, as discussed briefly in the Appendix, are given in (cf. [**9**]) after fitting the model to experimental data. They are written in the caption of Fig. 7,

For the bulk diffusion process we let $D = 0.2$, $\tau = 0.5$, and $L = 1$. For this case where $L/\sqrt{D} \approx 2.2$, the analytical stability results for the infinite-domain problem do not accurately predict the stability thresholds for this finite-domain problem. For the parameter values in Fig. 7, we calculate that

$$b \equiv -F_u^e > 0\,, \qquad F_c^e < 0\,, \qquad G_u^e < 0\,, \qquad G_c^e < 0\,.$$

In the right panel of Fig. 7 we show that $[\arg\,\mathcal{G}]\,\big|_{\Gamma_{I_+}} = 7\pi/4$. Since $b > 0$, we conclude from (3.13) that $N = 2$. Our full numerical simulations of the PDE-ODE system in the left panel of Fig. 7, showing an oscillatory dynamics, is consistent with this prediction. For the parameter values in the caption of Fig. 7 we have $a = 1.4223$, $b = 1.1525$, and $c = 0.2205$. We remark that since $b > 0$ and $c/b < 1 < a$, Proposition 3.5 proves that there is a Hopf bifurcation value of τ for the corresponding infinite-line problem given by $\tau_H \approx 0.5745$.

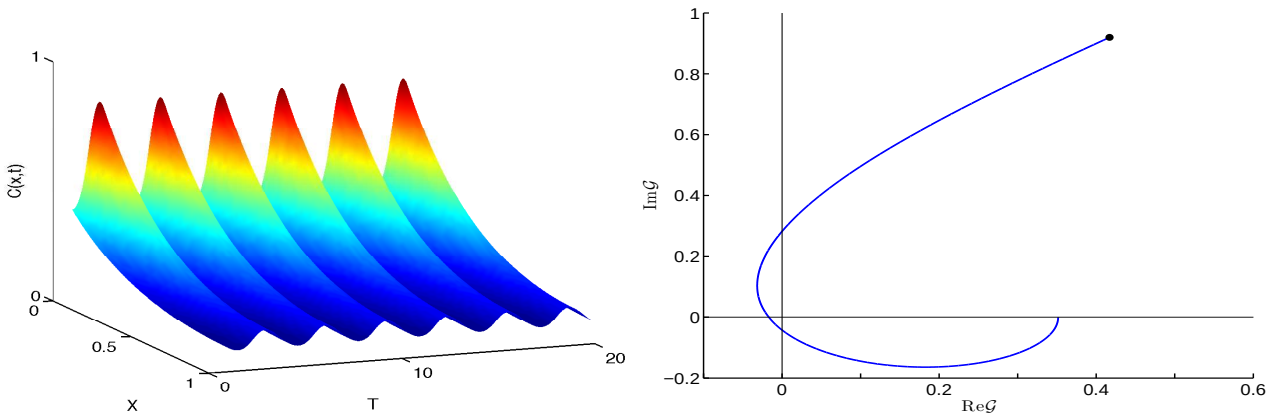

Figure 7. Left figure: Numerical results, showing oscillatory dynamics, for $C(x,t)$ in the *Dictyostelium* model (4.13). The bulk diffusion parameters are $D = 0.2$, $\tau = 0.5$, and $L = 1$. The parameters in the membrane-bulk coupling and dynamics in (4.13) are $\sigma^\star = 32$, $\alpha = 1.3$, $\Lambda = 0.005$, $\theta = 0.1$, $\epsilon = 0.2$, $k_1 = 1.125$, $L_1 = 316.228$, $k_2 = 0.45$, $L_2 = 0.03$, and $c_d = 100$. Right figure: Plot of the imaginary part versus the real part of $\mathcal{G}(i\omega)$ when $\lambda = i\omega$ and ω decreases from 100 (black dot) to 0. This shows that $[\arg\,\mathcal{G}]\,\big|_{\Gamma_{I_+}} = 7\pi/4$, and so $N = 2$ from (3.13).

The parameters used in Fig. 7 are adopted from [**9**] (page 245) except for the values of Λ, θ, α and σ. In Fig. 8 we plot the numerically computed bifurcation diagram of steady-state solutions for (4.13) as D is varied, together with the branches of synchronous periodic solutions. In the left panel of Fig. 8 we took $\Lambda = 0.005$, $\theta = 0.1$ and $\tau = 1.3$, corresponding

to Fig. 7, while in the right panel of Fig. 8 we took $\Lambda = 0.01$, $\theta = 0.01$ and $\tau = 1.2$. For the latter parameter set, the steady-state bifurcation diagram has an S-shaped bifurcation structure.

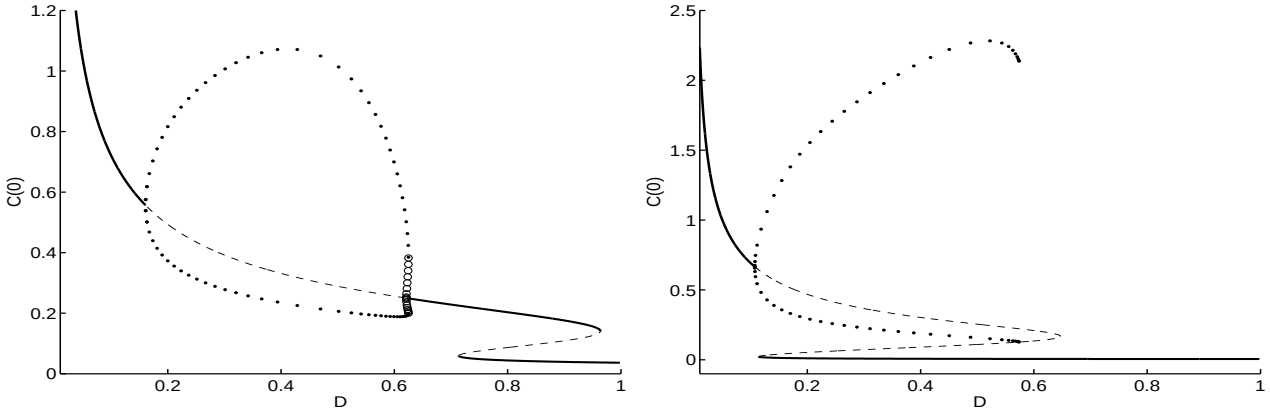

Figure 8. Bifurcation diagram of steady-state and synchronous periodic solution branches for the *Dictyostelium* model (4.13) with respect to the diffusivity D. The vertical axis is $C(0)$. Left panel: $\Lambda = 0.005$, $\theta = 0.1$ and $\tau = 1.3$. Right panel: $\Lambda = 0.01$, $\theta = 0.01$ and $\tau = 1.2$. In both panels the other parameter values used are the same as in Fig. 7. The solid/dashed lines denote stable/unstable branches of steady-state solutions. The solid/open circles indicates stable/unstable periodic solution branches of the synchronous mode. For the value $D = 0.2$ used in in the left panel of Fig. 7, we observe from the left panel above that the steady-state solution is unstable (as expected).

5 Two-Component Membrane Dynamics: Extension of the Basic Model

In our analysis so far we have assumed that the two membranes are identical. We now extend our analysis to allow for the more general case where the two membranes have possibly different dynamics. From the laboratory experiments of Pik-Yin Lai [**16**], it was observed for a certain two-cell system that one cell can have oscillatory dynamics, while the other cell is essentially quiescent. To illustrate such a behavior theoretically, we now modify our previous analysis to remove the assumed symmetry of the bulk concentration about the midline at $x = L$, and instead consider the whole system on $0 < x < 2L$. Allowing for the possibility of heterogeneous membranes, we consider

$$\begin{aligned} \tau C_t = DC_{xx} - C\,, \qquad t > 0\,, \quad 0 < x < 2L\,, \\ DC_x(0,t) = G_1(C(0,t),u_1)\,, \qquad DC_x(2L,t) = G_2(C(2L,t),v_1)\,. \end{aligned} \tag{5.1 a}$$

Here $C(x,t)$ is the bulk concentration of the signal, while u_1 and v_1 are their concentrations at the two membranes $x = 0$ and $x = 2L$, respectively. Inside each membrane, we assume the two-component dynamics

$$\begin{aligned} \frac{du_1}{dt} &= f_1(u_1,u_2) + \beta_1 \mathcal{P}(C(0,t),u_1)\,, \qquad \frac{du_2}{dt} = g(u_1,u_2)\,, \\ \frac{dv_1}{dt} &= f_2(v_1,v_2) + \beta_2 \mathcal{P}(C(2L,t),v_1)\,, \qquad \frac{dv_2}{dt} = g(v_1,v_2)\,, \end{aligned} \tag{5.1 b}$$

where the functions G_1, G_2, f_1, f_2, $\mathcal{P}$, and g are given by

$$\begin{aligned} G_1(C(0,t),u_1) &= \kappa_1\left[C(0,\ t) - u_1(t)\right]\,, \qquad G_2(C(2L,t),v_1) = \kappa_2\left[v_1(t) - C(2L,\ t)\right]\,, \\ f_1(u_1,u_2) &= \sigma_1 u_2 - q_1 u_1 - q_2 \frac{u_1}{1 + q_3 u_1 + q_4 u_1^2}\,, \qquad f_2(v_1,v_2) = \sigma_2 v_2 - p_1 v_1 - p_2 \frac{v_1}{1 + p_3 v_1 + p_4 v_1^2}\,, \\ g(\theta,\xi) &= \frac{1}{1+\theta^4} - \xi\,, \qquad \mathcal{P}(\theta,\xi) = \theta - \xi\,. \end{aligned} \tag{5.1 c}$$

This system, adopted from the key survey paper [**24**] for the design of realistic biological oscillators (see equation (8) of [**24**]), models a gene expression process and protein production for a certain biological system. With our choices of G_i for $i = 1, 2$ and $\mathcal{P}$, we have assumed a linear coupling between the bulk and the two membranes. The parameter values for σ, q_i and p_i, for $i = 1, \ldots, 3$, used below in our simulations are the same as in Fig. 3 of [**24**].

A simple calculation shows that the steady-state concentrations u_{1e}, u_{2e}, v_{1e}, and v_{2e}, satisfy the nonlinear algebraic system

$$\begin{aligned} &\frac{\sigma_1}{1+u_{1e}^4} - q_1 u_{1e} - \frac{q_2 u_{1e}}{1+q_3 u_{1e}+q_4 u_{1e}^2} + \beta_1(a_e u_{1e} + b_e v_{1e} - u_{1e}) = 0\,, \\ &\frac{\sigma_2}{1+v_{1e}^4} - p_1 v_{1e} - \frac{p_2 v_{1e}}{1+p_3 v_{1e}+p_4 v_{1e}^2} + \beta_2(c_e u_{1e} + d_e v_{1e} - v_{1e}) = 0\,, \end{aligned} \tag{5.2}$$

where we have defined a_e, b_e, c_e, and d_e, by

$$\begin{aligned} &a_e \equiv \kappa_1\delta^{-1}\left[D\omega_0\coth(2L\omega_0)+\kappa_2\right], \qquad b_e \equiv \kappa_2\delta^{-1}D\omega_0\,\mathrm{csch}(2L\omega_0)\,, \qquad c_e \equiv \kappa_1\delta^{-1}D\omega_0\,\mathrm{csch}(2L\omega_0)\,, \\ &d_e \equiv \kappa_2\delta^{-1}\left[D\omega_0\coth(2L\omega_0)+\kappa_1\right], \qquad \delta \equiv D^2\omega_0^2 + D\omega_0\left(\kappa_1+\kappa_2\right)\coth(2L\omega_0)+\kappa_1\kappa_2\,, \end{aligned} \tag{5.3}$$

where $\omega_0 \equiv D^{-1/2}$. In terms of u_{1e}, v_{1e}, u_{2e}, and v_{2e}, we have

$$C_e(0) = a_e u_{1e} + b_e v_{1e}\,, \qquad u_{2e} = \frac{1}{1+u_{1e}^4}\,, \qquad C_e(2L) = c_e u_{1e} + d_e v_{1e}\,, \qquad v_{2e} = \frac{1}{1+v_{1e}^4}\,. \tag{5.4}$$

To examine the stability of this steady-state solution, we introduce $C(x,t) = C_e(x) + e^{\lambda t}\eta(x)$, together with

$$u_1(t) = u_{1e} + e^{\lambda t}\phi_1\,, \qquad u_2(t) = u_{2e} + e^{\lambda t}\phi_2\,, \qquad v_1(t) = v_{1e} + e^{\lambda t}\psi_1\,, \qquad v_2(t) = v_{2e} + e^{\lambda t}\psi_2\,.$$

Upon linearizing (5.1), we obtain after some algebra that the eigenvalue λ satisfies the transcendental equation

$$\det\begin{pmatrix} \lambda - f_{1u_1} - \frac{f_{1u_2}g_{u_1}}{\lambda - g_{u_2}} + \beta_1 - \beta_1\mathcal{A}, & -\beta_1\mathcal{B} \\ -\beta_2\mathcal{C}, & \lambda - f_{2v_1} - \frac{f_{2v_2}g_{v_1}}{\lambda - g_{v_2}} + \beta_2 - \beta_2\mathcal{D} \end{pmatrix} = 0\,. \tag{5.5}$$

In (5.5) we have labeled $g_{u_1} \equiv \partial_{u_1} g(u_1, u_2)$, $g_{u_2} \equiv \partial_{u_2} g(u_1, u_2)$, $g_{v_1} \equiv \partial_{v_1} g(v_1, v_2)$, and $g_{v_2} \equiv \partial_{v_2} g(v_1, v_2)$. Moreover, we have defined $\mathcal{A}$, $\mathcal{B}$, $\mathcal{C}$, and $\mathcal{D}$, by

$$\begin{aligned} &\mathcal{A} \equiv \kappa_1\Delta^{-1}\left[\kappa_2 + D\Omega_\lambda\coth(2L\Omega_\lambda)\right], \qquad \mathcal{B} \equiv \kappa_2\Delta^{-1}D\Omega_\lambda\,\mathrm{csch}(2L\Omega_\lambda)\,, \qquad \mathcal{C} \equiv \kappa_1\Delta^{-1}D\Omega_\lambda\,\mathrm{csch}(2L\Omega_\lambda)\,, \\ &\mathcal{D} \equiv \kappa_2\Delta^{-1}\left[\kappa_1 + D\Omega_\lambda\coth(2L\Omega_\lambda)\right], \qquad \Delta \equiv D^2\Omega_\lambda^2 + \kappa_1\kappa_2 + \left(\kappa_1+\kappa_2\right)D\Omega_\lambda\coth(2L\Omega_\lambda)\,. \end{aligned}$$

Here $\Omega_\lambda \equiv \sqrt{\frac{1+\tau\lambda}{D}}$ and f_{is_j} denote partial derivatives of f_i where $i = 1, 2$ with respect to s_j, $s = u, v$ and $j = 1, 2$.

When there are two identical membranes, the eigenvector of the matrix in (5.5) corresponding to the eigenvalue at the stability threshold is either $(1,1)^T$ (in-phase synchronization) or $(1,-1)^T$ (anti-phase synchronization). For this identical membrane case where $\beta \equiv \beta_1 = \beta_2$, in the left panel of Fig. 9 we plot the numerically computed bifurcation diagram in terms of β, showing the possibility of either synchronous or asynchronous oscillatory dynamics in the two membranes. In the right panel of Fig. 9 we plot the full numerical solution computed from the PDE-ODE system (5.1) when $\beta = 0.4$, which reveals a synchronous oscillatory instability. The parameter values used in the simulation are given in the caption of Fig. 9. To determine the number N of eigenvalues of the linearization in $\mathrm{Re}(\lambda) > 0$ for the identical membrane case, where $f_1 = f_2 \equiv f$, we recall that λ must be a root of (2.14). As such, we seek roots of $\mathcal{G}(\lambda) = 0$ in $\mathrm{Re}(\lambda) > 0$, where

$$\mathcal{G}(\lambda) \equiv \frac{1}{p_\pm(\lambda)} - \frac{(g_{u_2}-\lambda)}{\det\left(J_e - \lambda I\right)}\,, \qquad J_e \equiv \begin{pmatrix} \left.\frac{\partial f}{\partial u_1}\right|_{\boldsymbol{u}=\boldsymbol{u}_e}, & \left.\frac{\partial f}{\partial u_2}\right|_{\boldsymbol{u}=\boldsymbol{u}_e} \\ \left.\frac{\partial g}{\partial u_1}\right|_{\boldsymbol{u}=\boldsymbol{u}_e}, & \left.\frac{\partial g}{\partial u_2}\right|_{\boldsymbol{u}=\boldsymbol{u}_e} \end{pmatrix}. \tag{5.6}$$

Here $p_+(\lambda)$ and $p_-(\lambda)$ are defined in (2.6) and (2.8), respectively. For our example we find that $p_\pm(\lambda)$ is non-vanishing

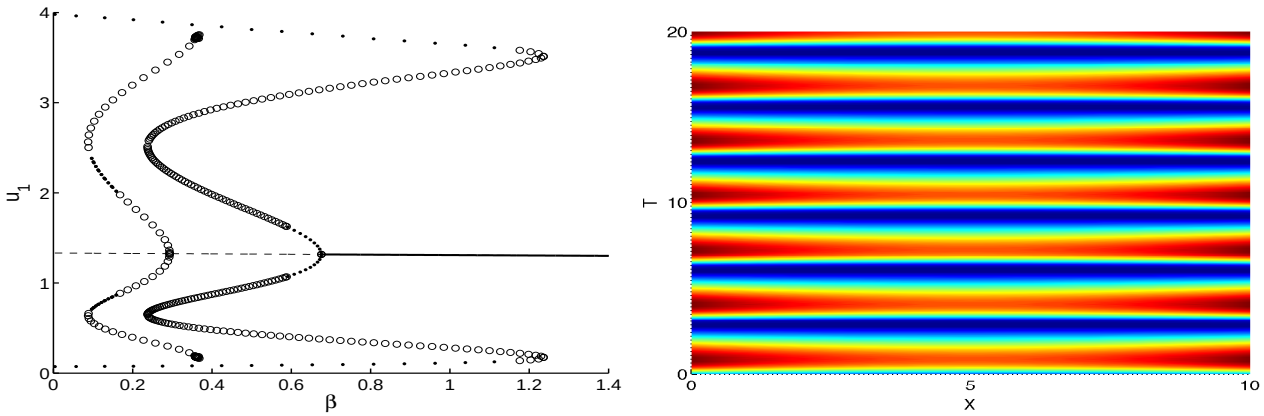

Figure 9. Left panel: Bifurcation diagram with respect to β in the two identical membrane case. The larger and smaller values of β at the two Hopf bifurcation points correspond to the synchronous and asynchronous modes respectively. The branches of periodic solutions corresponding to synchronous and asynchronous oscillations are shown. There are secondary instabilities bifurcating from these branches that are not shown. The solid/open circles indicates stable/unstable portions of the periodic solution branches. The parameter values for bulk diffusion are $D = 50$, $\tau = 0.1$, and $L = 5$, while the parameter values for the membrane dynamics are identical for both membranes and are fixed at $p_1 = q_1 = 1$, $p_2 = q_2 = 200$, $p_3 = q_3 = 10$, $p_4 = q_4 = 35$, $\sigma_1 = \sigma_2 = 20$, and $\kappa_1 = \kappa_2 = 20.0$. Right panel: Full numerical solution of the PDE-ODE system (5.1) when $\beta = 0.4$, revealing a synchronous oscillatory instability.

in $\mathrm{Re}(\lambda) > 0$. Then, by using the argument principle as in the proof of Lemma 3.1, and noting that $\mathcal{G}(\lambda)$ is bounded as $|\lambda| \to +\infty$ in $\mathrm{Re}(\lambda) > 0$, we obtain that

$$N = P + \frac{1}{\pi} \left[\arg\, \mathcal{G}\right]\big|_{\Gamma_{I_+}} . \tag{5.7}$$

Here P is the number of roots of $\det(J_e - \lambda I) = 0$ (counting multiplicity) in $\mathrm{Re}(\lambda) > 0$, and $\left[\arg\, \mathcal{G}\right]\big|_{\Gamma_{I_+}}$ denotes the change in the argument of $\mathcal{G}(\lambda)$ along the semi-infinite imaginary axis $\lambda = i\omega$ with $0 < \omega < \infty$, traversed in the downwards direction. In Fig. 10 we show a numerical computation of the winding number (5.7) near the values of β at the bifurcation points of the synchronous and asynchronous solution branches shown in the left panel of Fig. 9.

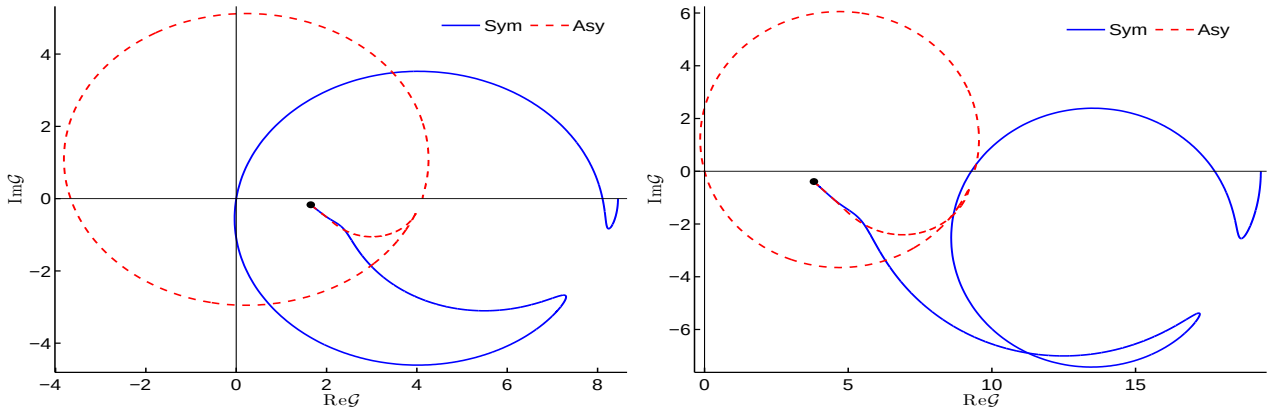

Figure 10. Winding number computation verifying the location of the Hopf bifurcation point of the synchronous mode (left panel $\beta = 0.6757$) and the asynchronous mode (right panel $\beta = 0.2931$) corresponding to the bifurcation diagram shown in the left panel of Fig. 9. The other parameter values are as given in the caption of Fig. 9. The formula (5.7) determines the number N of unstable eigenvalues in $\mathrm{Re}(\lambda) > 0$. For both plots $P = 2$ in (5.7). When the change in the argument of $\mathcal{G}(i\omega)$ is -2π, then $N = 0$. Otherwise if the change in the argument is 0, then $N = 2$.

However, when the two membranes are not identical, the matrix in (5.5) can have eigenvectors that are close to $(1,0)^T$ or $(0,1)^T$, which corresponds to a large difference in the amplitude of the oscillations in the two membranes. In such a case, we will observe a prominent oscillation in only one of the two membranes. We choose the coupling strengths β_1 and β_2 to be the bifurcation parameters, and denote μ by $\mu \equiv \beta_2 - \beta_1$. The other parameter values in the model are taken to be the identical for the two membranes. To illustrate that a large oscillation amplitude ratio between the two membranes can occur, in Fig. 11 we show full numerical results from the PDE-ODE system (5.1) with $D = 1$ when $\beta_1 = 0.2$ and $\beta_2 = 0.7$. From this figure we observe that the concentration of the signaling molecule undergoes a large amplitude oscillation near one boundary and a significantly smaller amplitude oscillation near the other boundary.

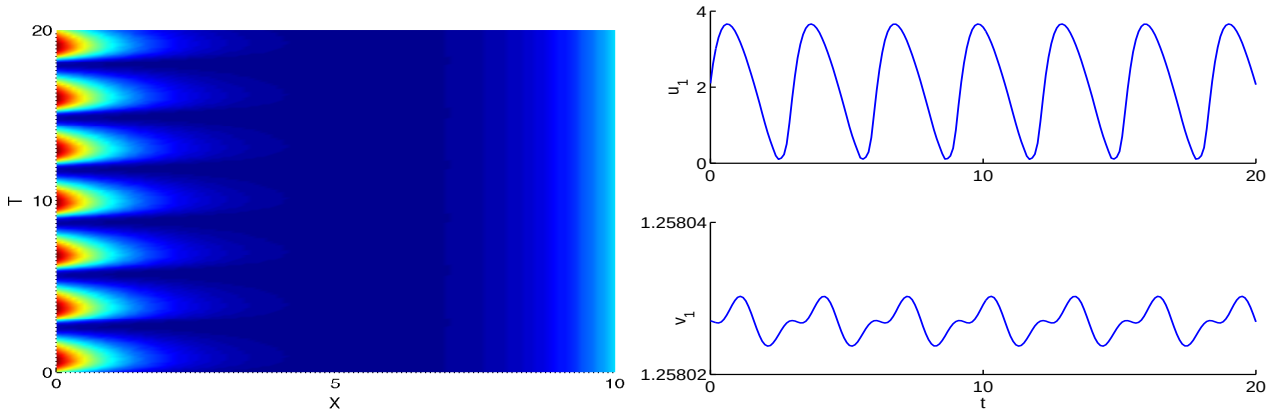

Figure 11. Left panel: plot of the oscillatory instability for the case of heterogeneous membranes as computed from the PDE-ODE system (5.1) with $D = 1$, $\kappa_1 = \kappa_2 = 0.1$, and with the same parameters as in the caption of Fig. 9. The two membranes differ only in their coupling strengths with $\beta_1 = 0.2$ and $\beta_2 = 0.7$. The oscillation is pronounced only in the membrane at $x = 0$, with only a very small-scale oscillation in the second membrane at $x = 2L$ with $L = 5$. Right panel: similar plot showing u_1 (left boundary) and v_1 (right boundary) versus t, showing the large amplitude difference.

6 Weakly Nonlinear Theory for Synchronous Oscillations

In §3 we showed that, depending on the nature of the membrane-bulk coupling mechanism, spatial-temporal oscillations are possible for a membrane-bulk model consisting of a single species on each membrane that is coupled through linear bulk diffusion. These oscillations originate from a Hopf bifurcation associated with the symmetric steady-state solution branch. In this section we develop a weakly nonlinear analysis in the vicinity of this Hopf bifurcation, which leads to an amplitude equation characterizing small amplitude oscillations. By evaluating the coefficients in this amplitude equation, we determine whether the Hopf bifurcation is supercritical or subcritical. This asymptotic prediction for the stationary periodic solution near the bifurcation point is then compared favorably with full numerical results for a specific system.

We illustrate our weakly nonlinear theory only for the case of synchronous oscillations. The resulting model, assuming only one species on the membrane, is formulated as

$$C_{xx} - \frac{1}{D}C = \frac{\tau}{D}C_t\,, \qquad t>0\,, \quad 0<x<L\,; \qquad C_x(L,t) = 0\,; \qquad DC_x\big|_{x=0} = G(C(0,t),u)\,, \tag{6.1 a}$$

with the local membrane dynamics

$$\frac{du}{dt} = F(C(0,t),u(t))\,. \tag{6.1 b}$$

The steady-state solution $(C_e(x), u_e)$ of (6.1) satisfies

$$\begin{aligned} \partial_{xx} C_e - \frac{1}{D} C_e = 0\,, \qquad 0 < x < L\,; \qquad \partial_x C_e(L) = 0\,, \\ D\partial_x C_e(0) = G(C_e(0), u)\,, \qquad F\left(C_e(0), u_e\right) = 0\,. \end{aligned} \tag{6.2}$$

We choose the diffusivity D as the bifurcation parameter. We assume that when $D = D_0$ the linearization of (6.1) around the steady-state solution has a complex conjugate pair of imaginary eigenvalues, and that all the other eigenvalues of the linearization satisfy $\mathrm{Re}(\lambda) < 0$.

We will analyze the weakly nonlinear dynamics of (6.1) when D is close to D_0. As such, we introduce $\epsilon \ll 1$ and a detuning-parameter D_1 by $D = D_0 + \epsilon^2 D_1$, with $D_1 = \pm 1$ indicating the direction of the bifurcation, so that

$$D = D_0 + \epsilon^2 D_1\,, \qquad \frac{1}{D} = \frac{1}{D_0 + \epsilon^2 D_1 + \mathcal{O}(\epsilon^4)} = \frac{1}{D_0} - \epsilon^2 \frac{D_1}{D_0^2} + \mathcal{O}(\epsilon^4)\,. \tag{6.3}$$

To derive the amplitude equation, we will employ a formal two time-scale asymptotic method where we introduce the slow time $T = \epsilon^2 t$, so that $d/dt = \partial/\partial t + \epsilon^2 \partial/\partial T$. For $D - D_0 = \mathcal{O}(\epsilon^2)$, we then expand the solution to (6.1) as

$$\begin{aligned} C(x,t,T) = C_e(x) + \epsilon C_1(x,t,T) + \epsilon^2 C_2(x,t,T) + \epsilon^3 C_3(x,t,T) + \dots\,, \\ u(t,T) = u_e + \epsilon u_1(t,T) + \epsilon^2 u_2(t,T) + \epsilon^3 u_3(t,T) + \dots\,. \end{aligned} \tag{6.4}$$

We then substitute (6.4) into (6.1) and equate powers of ϵ.

To leading-order in ϵ, we obtain the steady-state problem (6.2) when $D = D_0$. This has the solution

$$C_e(x) = C_e^0 \frac{\cosh\left[\omega_0 (L - x)\right]}{\cosh(\omega_0 L)}\,, \qquad \omega_0 \equiv 1/\sqrt{D_0}\,, \tag{6.5 a}$$

with $C_e^0 \equiv C_e(0)$, where the constants C_e^0 and u_e are determined from the nonlinear algebraic system

$$-C_e^0 \tanh(\omega_0 L) = \omega_0 G(C_e^0, u_e)\,, \qquad F(C_e^0, u_e) = 0\,. \tag{6.5 b}$$

The $\mathcal{O}(\epsilon)$ system is the linearization of (6.1) around the steady-state solution, which is written as

$$\begin{aligned} C_{1xx} - \frac{1}{D_0} C_1 = \frac{\tau}{D_0} C_{1t}\,, \qquad t > 0\,, \quad 0 < x < L\,; \qquad C_{1x}(L,t,T) = 0\,, \\ D_0 C_{1x}\big|_{x=0} = C_1 G_c^e + u_1 G_u^e\,, \quad \text{on } x = 0\,, \\ u_{1t} = C_1 F_c^e + u_1 F_u^e\,, \quad \text{on } x = 0\,. \end{aligned} \tag{6.6}$$

Here F_j^e, G_j^e denote partial derivatives of F or G with respect to i evaluated at the steady-state solution $(C_e(0), u_e)$ at $x = 0$, where $j = \{C, u\}$. At $\mathcal{O}(\epsilon^2)$, we have that $C_2(x,t,T)$ and $u_2(t,T)$ satisfy

$$\begin{aligned} C_{2xx} - \frac{1}{D_0} C_2 = \frac{\tau}{D_0} C_{2t} - \frac{D_1}{D_0^2} C_e\,, \qquad t > 0\,, \quad 0 < x < L\,; \qquad C_{2x}(L,t,T) = 0\,, \\ D_0 C_{2x}\big|_{x=0} = C_2 G_c^e + u_2 G_u^e + \frac{1}{2}\left(C_1^2 G_{cc}^e + u_1^2 G_{uu}^e + 2 C_1 u_1 G_{cu}^e\right) - \frac{D_1}{D_0} G^e\,, \quad \text{on } x = 0\,, \\ u_{2t} = C_2 F_c^e + u_2 F_u^e + \frac{1}{2}\left(C_1^2 F_{cc}^e + u_1^2 F_{uu}^e + 2 C_1 u_1 F_{cu}^e\right)\,, \quad \text{on } x = 0\,. \end{aligned} \tag{6.7}$$

In a similar notation, F_{cc}^e denotes the second partial derivative of F with respect to C evaluated at the steady-state pair

$(C_e(0), u_e)$. Lastly, the $\mathcal{O}(\epsilon^3)$ system for $C_3(x,t,T)$ and $u_3(t,T)$, where resonances will first appear, is

$$\begin{aligned}
&C_{3xx} - \frac{1}{D_0}C_3 = \frac{\tau}{D_0}C_{3t} - \frac{D_1}{D_0^2}C_1 - \frac{D_1\tau}{D_0^2}C_{1t} + \frac{\tau}{D_0}C_{1T}\,, \qquad t>0\,, \quad 0<x<L\,; \qquad C_{3x}(L,t,T) = 0\,,\\
&D_0 C_{3x}\big|_{x=0} = C_3 G_c^e + u_3 G_u^e + C_1C_2G_{cc}^e + u_1u_2G_{uu}^e + (C_1u_2 + C_2u_1)\,G_{cu}^e\\
&\qquad\qquad + \frac{1}{6}\left(C_1^3G_{ccc}^e + 3C_1^2u_1G_{ccu}^e + 3C_1u_1^2G_{cuu}^e + u_1^3G_{uuu}^e\right) - \frac{D_1}{D_0}\left(C_1G_c^e + u_1G_u^e\right)\,, \quad \text{on } x=0\,,\\
&u_{3t} = -u_{1T} + C_3F_c^e + u_3F_u^e + C_1C_2F_{cc}^e + u_1u_2F_{uu}^e + (C_1u_2 + C_2u_1)\,F_{cu}^e\\
&\qquad\qquad + \frac{1}{6}\left(C_1^3F_{ccc}^e + 3C_1^2u_1F_{ccu}^e + 3C_1u_1^2F_{cuu}^e + u_1^3F_{uuu}^e\right)\,, \quad \text{on } x=0\,.
\end{aligned} \tag{6.8}$$

When $D = D_0$, (6.6) is assumed to have a complex conjugate pair of pure imaginary eigenvalues, and so we write

$$C_1(x,t,T) = A(T)e^{i\lambda_I t}\eta_0(x) + \text{c.c.}\,, \qquad u_1(t,T) = A(T)e^{i\lambda_I t}\phi_0 + \text{c.c.}\,, \tag{6.9}$$

for some $\lambda_I > 0$. Here $\eta_0(x)$ and ϕ_0 is the eigenpair associated with the linearized problem, and c.c. denotes the complex conjugate. An ODE for the unknown complex amplitude $A(T)$ will be derived by imposing a non-resonance condition on the $\mathcal{O}(\epsilon^3)$ system (6.8). To normalize the eigenpair, we impose for convenience that $\eta_0(0) = 1$.

Upon substituting (6.9) into (6.6), we obtain that $\eta_0(x)$ and ϕ_0 satisfy

$$\begin{aligned}
&\eta_0'' - \frac{(1+i\lambda_I\tau)}{D_0}\eta_0 = 0\,, \qquad 0<x<L\,; \qquad D_0\eta_{0x}(0) = G_c^e\eta_0(0) + G_u^e\phi_0\,, \quad \eta_{0x}(L) = 0\,,\\
&F_c^e\eta_0(0) + F_u^e\phi_0 = i\lambda_I\phi_0\,, \quad \text{on } x=0\,.
\end{aligned} \tag{6.10}$$

We solve this system, and impose the normalization $\eta_0(0) = 1$, to obtain

$$\eta_0(x) = \frac{\cosh\left[\Omega_\lambda(L-x)\right]}{\cosh(\Omega_\lambda L)}\,, \qquad \phi_0 = \frac{F_c^e}{i\lambda_I - F_u^e}\,, \qquad \Omega_\lambda \equiv \sqrt{\frac{1+i\tau\lambda_I}{D_0}}\,, \tag{6.11}$$

where we must take the principal value of the square root. From the condition for η_{0x} on $x=0$ in (6.10), we obtain that $i\lambda_I$ is a root of the following transcendental equation, which occurs at the critical value D_0 of D:

$$\left(D_0\Omega_\lambda\tanh(\Omega_\lambda L) + G_c^e\right)\left(i\lambda_I - F_u^e\right) + F_c^eG_u^e = 0\,. \tag{6.12}$$

The spectral problem (6.10) is a nonstandard eigenvalue problem since the eigenvalue parameter appears in both the differential operator as well as in the boundary condition on $x=0$. Therefore, we cannot simply define the operator $\mathcal{L} = \frac{D_0}{\tau}\frac{d^2}{dx^2} - \frac{1}{\tau}$ and consider the problem as a special case of $\mathcal{L}u = \lambda u$, owing to the fact that the domain of $\mathcal{L}$ depends on λ. Instead, we must extend our definition of $\mathcal{L}$, construct its adjoint and find an expansion theorem following the approach in [**8**] for treating non self-adjoint spectral problems with an eigenvalue-dependent boundary condition. This formalism will then allow for a systematic imposition of a solvability condition on the $\mathcal{O}(\epsilon^3)$ problem (6.8), which leads to the amplitude equation for $A(T)$.

Motivated by the form of (6.10), we define an operator $\mathcal{L}$ acting on a two-component vector $U \equiv (u(x),\ u_1)^T$ by

$$\mathcal{L}\begin{pmatrix} u(x) \\ u_1 \end{pmatrix} \equiv \begin{pmatrix} \frac{D_0}{\tau}u''(x) - \frac{1}{\tau}u(x) \\ F_c^eu(0) + F_u^eu_1 \end{pmatrix}\,, \tag{6.13 a}$$

where $u(x)$ satisfies the boundary conditions

$$u_x(L) = 0\,, \qquad D_0u_x(0) = G_c^eu(0) + G_u^eu_1\,. \tag{6.13 b}$$

The calculation in (6.11) shows that $\mathcal{L}U = i\lambda_I U$, with normalization $u(0) = 1$, where U is given by

$$U = \begin{pmatrix} \frac{\cosh[\Omega_\lambda(L-x)]}{\cosh(\Omega_\lambda L)} \\ \frac{F_c^e}{i\lambda_I - F_u^e} \end{pmatrix}. \tag{6.14}$$

Next, we define an inner product of two vectors $U \equiv (u(x),\ u_1)^T$ and $V \equiv (v(x),\ v_1)^T$ by

$$\langle U, V\rangle \equiv \int_0^L u(x)\overline{v}(x)\,dx + u_1\overline{v}_1\,, \tag{6.15}$$

where the overbar denotes complex conjugate, and where we restrict our attention to the subspace where

$$u_x(L) = 0\,, \qquad D_0 u_x(0) = G_c^e u(0) + G_u^e u_1\,. \tag{6.16}$$

With this definition of the inner product, we integrate by parts to establish that $\langle \mathcal{L}U, V\rangle = \langle U, \mathcal{L}^\star V\rangle$, in terms of an adjoint operator $\mathcal{L}^\star$ defined by

$$\mathcal{L}^\star V \equiv \begin{pmatrix} \frac{D_0}{\tau}v''(x) - \frac{1}{\tau}v(x) \\ F_u^e v_1 - G_u^e v(0)/\tau \end{pmatrix}. \tag{6.17}$$

Here V is a two-component vector satisfying the adjoint boundary conditions

$$v_x(L) = 0\,, \qquad D_0 v_x(0) = G_c^e v(0) - \tau F_c^e v_1\,. \tag{6.18}$$

A simple calculation shows that $-i\lambda_I$ is also an eigenvalue of $\mathcal{L}^\star$ (as expected), and that the eigenvector satisfying the adjoint problem $\mathcal{L}^\star V = -i\lambda_I V$, normalized by $v(0) = 1$, and where Ω_λ is defined in (6.11), is

$$V = \begin{pmatrix} \frac{\cosh\left[\overline{\Omega}_\lambda(L-x)\right]}{\cosh(\overline{\Omega}_\lambda L)} \\ \frac{G_u^e}{\tau(F_u^e + i\lambda_I)} \end{pmatrix}. \tag{6.19}$$

With the determination of the solution to (6.6) now complete, we then proceed to the $\mathcal{O}(\epsilon^2)$ system (6.7). We substitute (6.9) into (6.7) and separate variables to conclude that $C_2(x,t,T)$ and $u_2(t,T)$ must have the form

$$\begin{aligned} C_2(x,t,T) &= g_0(x,T) + g_1(x,T)e^{i\lambda_I t} + g_2(x,T)e^{2i\lambda_I t} + \text{c.c.}\,, \\ u_2(t,T) &= h_0(T) + h_1(T)e^{i\lambda_I t} + h_2(T)e^{2i\lambda_I t} + \text{c.c.}\,, \end{aligned} \tag{6.20}$$

where $g_j(x,T)$ and $h_j(T)$ for $j = 0,1,2$ are to be determined. Since the problem for g_1 and h_1 is simply the linearized problem (6.6), without loss of generality we can take $g_1 \equiv 0$ and $h_1 \equiv 0$. By comparing terms independent of powers of $e^{i\lambda_I t}$, we conclude, upon using $\eta_0(0) = 1$, that g_0 and h_0 are real-valued and satisfy

$$\begin{aligned} g_{0xx} - \frac{1}{D_0}g_0 &= -\frac{D_1}{D_0^2}C_e\,, \qquad 0 < x < L\,; \qquad g_{0x}(L) = 0\,, \\ Dg_{0x}(0) - (g_0(0)G_c^e + h_0 G_u^e) &= |A|^2\frac{\Pi_2}{2} - \frac{D_1}{D_0}G^e\,, \quad \text{on } x = 0\,, \\ g_0(0)F_c^e + h_0 F_u^e &= -|A|^2\frac{\Delta_2}{2} \quad \text{on } x = 0\,. \end{aligned} \tag{6.21 a}$$

In the notation in (6.21 a) we have suppressed the dependence of g_0 on T. Here we have defined Π_2 and Δ_2 by

$$\Pi_2 \equiv 2G_{cc}^e + 2|\phi_0|^2 G_{uu}^e + 4\text{Re}(\phi_0)G_{cu}^e\,, \qquad \Delta_2 \equiv 2F_{cc}^e + 2|\phi_0|^2 F_{uu}^e + 4\text{Re}(\phi_0)F_{cu}^e\,, \tag{6.21 b}$$

where $|z|$ denotes the modulus of z. In a similar way, upon comparing $e^{2i\lambda_I t}$ terms, we obtain that g_2 and h_2 satisfy

$$\begin{aligned} &g_{2xx} - \frac{(1+2i\tau\lambda_I)}{D_0} g_2 = 0\,, \qquad 0 < x < L\,; \qquad g_{2x}(L) = 0\,, \\ &Dg_{2x}(0) - (g_2(0)G_c^e + h_2 G_u^e) = |A|^2 \frac{\Pi_1}{2}\,, \quad \text{on } x = 0\,, \\ &g_2(0)F_c^e + h_2 F_u^e - 2i\lambda_I h_2 = -|A|^2 \frac{\Delta_1}{2} \quad \text{on } x = 0\,, \end{aligned} \tag{6.22 a}$$

and are complex-valued. Here, we have defined Π_1 and Δ_1 by

$$\Pi_1 \equiv G_{cc}^e + \phi_0^2 G_{uu}^e + 2\phi_0 G_{cu}^e\,, \qquad \Delta_1 \equiv F_{cc}^e + \phi_0^2 F_{uu}^e + 2\phi_0 F_{cu}^e\,. \tag{6.22 b}$$

Next, we solve the problem (6.21) for $g_0(x)$ and h_0 explicitly. Since the inhomogeneous term proportional to C_e in the differential operator for g_0 satisfies the homogeneous problem, we can readily determine the particular solution for (6.21 a). With this observation, and after some algebra, we obtain that

$$g_0 = g_0^1 \cosh\left[\omega_0(L-x)\right] + \frac{P_0 D_1 L}{2\omega_0} \sinh\left[\omega_0(L-x)\right] - \frac{P_0 D_1}{2\omega_0} x \sinh\left[\omega_0(L-x)\right]\,, \tag{6.23 a}$$

where $\omega_0 \equiv \sqrt{1/D_0}$ and P_0 is defined by

$$P_0 \equiv -\frac{C_e^0}{D_0^2 \cosh(\omega_0 L)}\,. \tag{6.23 b}$$

In (6.23 a), the constant g_0^1 is given by

$$g_0^1 = D_1\chi_1 + |A|^2\chi_2\,, \tag{6.23 c}$$

where χ_1 and χ_2 are defined in terms of Δ_2 and Π_2, given in (6.21 b), by

$$\chi_1 \equiv \frac{P_{03}G_u^e - P_{02}F_u^e}{P_{01}F_u^e - F_c^e G_u^e \cosh(\omega_0 L)}\,, \qquad \chi_2 \equiv \frac{1}{2}\left(\frac{\Delta_2 G_u^e - \Pi_2 F_u^e}{P_{01}F_u^e - F_c^e G_u^e \cosh(\omega_0 L)}\right)\,. \tag{6.23 d}$$

Here the three new quantities P_{01}, P_{02}, and P_{03}, are defined in terms of P_0 of (6.23 b), by

$$\begin{aligned} &P_{01} \equiv D_0\omega_0 \sinh(\omega_0 L) + G_c^e \cosh(\omega_0 L)\,, \qquad P_{03} \equiv F_c^e\left(\frac{P_0 L}{2\omega_0}\right)\sinh(\omega_0 L)\,, \\ &P_{02} \equiv \frac{P_0 L}{2\omega_0}\left[D_0\omega_0\cosh(\omega_0 L) + G_c^e \sinh(\omega_0 L)\right] + \frac{P_0 D_0}{2\omega_0}\sinh(\omega_0 L) - \frac{G^e}{D_0}\,. \end{aligned} \tag{6.23 e}$$

In addition, the real-valued constant h_0 is given by in terms of P_0, P_{01}, P_{02}, P_{03}, Π_2, and Δ_2, by

$$h_0 = D_1\chi_3 + |A|^2\chi_4\,, \tag{6.24 a}$$

where χ_3 and χ_4 are defined by

$$\chi_3 \equiv \frac{P_{02}F_c^e\cosh(\omega_0 L) - P_{01}P_{03}}{P_{01}F_u^e - G_u^e F_c^e \cosh(\omega_0 L)}\,, \qquad \chi_4 \equiv \frac{1}{2}\left(\frac{\Pi_2 F_c^e \cosh(\omega_0 L) - \Delta_2 P_{01}}{P_{01}F_u^e - G_u^e F_c^e \cosh(\omega_0 L)}\right)\,. \tag{6.24 b}$$

Finally, in our solvability condition for the amplitude equation to be derived below, we will need to evaluate g_0 at $x = 0$. Upon using (6.23 a) and (6.23 c), we can write $g_0(0)$ as

$$g_0(0) = D_1 g_{0c} + g_{0A}|A|^2\,; \qquad g_{0c} \equiv \chi_1\cosh(\omega_0 L) + \frac{P_0 L}{2\omega_0}\sinh(\omega_0 L)\,, \qquad g_{0A} \equiv \chi_2\cosh(\omega_0 L)\,. \tag{6.25}$$

Next, we solve the problem (6.22) for g_2 and h_2. We readily calculate that

$$g_2(x) = g_2^0 \frac{\cosh\left[\Omega_{2\lambda}(L-x)\right]}{\cosh(\Omega_{2\lambda}L)}\,, \qquad \Omega_{2\lambda} \equiv \sqrt{\frac{1+2i\tau\lambda_I}{D_0}}\,,$$

where g_2^0 and h_2 satisfy the 2×2 linear system

$$[D_0\Omega_{2\lambda}\tanh(\Omega_{2\lambda}L)+G_c^e]\,g_2^0+G_u^e h_2=-\frac{\Pi_1}{2}A^2\,,\qquad F_c^e g_2^0+(F_u^e-2i\lambda_I)\,h_2=-\frac{\Delta_1}{2}A^2\,.$$

Here Π_1 and Δ_1 are defined in (6.22 b). By solving this linear system, we obtain that

$$g_2(0)\equiv g_2^0=\chi_6 A^2\,,\qquad h_2=\chi_5 A^2\,, \tag{6.26 a}$$

where χ_5 and χ_6 are defined by

$$\begin{aligned}\chi_5&\equiv\frac{1}{2}\left(\frac{\Pi_1 F_c^e-\Delta_1(D_0\Omega_{2\lambda}\tanh(\Omega_{2\lambda}L)+G_c^e)}{(D_0\Omega_{2\lambda}\tanh(\Omega_{2\lambda}L)+G_c^e)\,(F_u^e-2i\lambda_I)-G_u^eF_c^e}\right),\\ \chi_6&\equiv\frac{1}{2}\left(\frac{\Pi_1(2i\lambda_I-F_u^e)+\Delta_1 G_u^e}{(D_0\Omega_{2\lambda}\tanh(\Omega_{2\lambda}L)+G_c^e)\,(F_u^e-2i\lambda_I)-G_u^eF_c^e}\right).\end{aligned} \tag{6.26 b}$$

With the solution of the $\mathcal{O}(\epsilon^2)$ system (6.7) complete, we now proceed to the $\mathcal{O}(\epsilon^3)$ problem (6.8), where the resonance term comes into play. We substitute the expression of C_1, u_1 and C_2, u_2 from (6.9) and (6.20), respectively, into (6.8), and identify all terms that are proportional to $e^{i\lambda_I t}$. In order to eliminate resonance in (6.8), thereby ensuring that $C_3(x,t,T)$ and $u_3(t,T)$ remain bounded on asymptotically long time intervals of order $t=\mathcal{O}(\epsilon^{-1})$, we require that the coefficients of the $e^{i\lambda_I t}$ terms satisfy a certain compatibility condition. This leads to an amplitude equation for $A(T)$.

To derive this amplitude equation, we substitute

$$\begin{aligned}C_3(x,t,T)&=\mathcal{C}_4(x,T)+\mathcal{C}_3(x,T)e^{i\lambda_I t}+\mathcal{C}_2(x,T)e^{2i\lambda_I t}+\mathcal{C}_1(x,T)e^{3i\lambda_I t}+\text{c.c.}\,,\\ u_3(t,T)&=U_4(T)+U_3(T)e^{i\lambda_I t}+U_2(T)e^{2i\lambda_I t}+U_2(T)e^{3i\lambda_I t}+\text{c.c.}\,,\end{aligned} \tag{6.27}$$

together with (6.9) and (6.20) into (6.8), to obtain, after a lengthy but straightforward calculation, that $\mathcal{C}_3$, U_3 satisfy

$$\mathcal{L}\begin{pmatrix}\mathcal{C}_3\\ U_3\end{pmatrix}\equiv\begin{pmatrix}\frac{D_0}{\tau}\mathcal{C}_{3xx}-\frac{1}{\tau}\mathcal{C}_3\\ F_c^e\mathcal{C}_3(0)+F_u^eU_3\end{pmatrix}=i\lambda_I\begin{pmatrix}\mathcal{C}_3\\ U_3\end{pmatrix}+\begin{pmatrix}\mathcal{R}_1\\ A'\phi_0-\mathcal{R}_3\end{pmatrix},\qquad 0<x<L\,, \tag{6.28 a}$$

where $\mathcal{C}_3(x)$ satisfies the boundary conditions

$$\mathcal{C}_{3x}(L)=0\,,\qquad D_0\mathcal{C}_{3x}\big|_{x=0}-[G_c^e\mathcal{C}_3(0)+G_u^eU_3]=\mathcal{R}_2\,. \tag{6.28 b}$$

In the notation of (6.28) we have suppressed the dependence of $\mathcal{C}_3$ on T. In (6.28), $\mathcal{R}_1$ is defined by

$$\mathcal{R}_1\equiv A'\eta_0-\frac{D_1}{D_0\tau}\,(1+i\tau\lambda_I)\,A\eta_0\,, \tag{6.29 a}$$

and the residuals $\mathcal{R}_2$ and $\mathcal{R}_3$ have the form

$$\mathcal{R}_2=D_1A\mathcal{R}_{20}+A|A|^2\mathcal{R}_{21}\,,\qquad \mathcal{R}_3=D_1A\mathcal{R}_{30}+A|A|^2\mathcal{R}_{31}\,. \tag{6.29 b}$$

The coefficients $\mathcal{R}_{20}$ and $\mathcal{R}_{30}$ of the linear term in A are

$$\begin{aligned}\mathcal{R}_{20}&\equiv g_{0c}G_{cc}^e+\phi_0\chi_3G_{uu}^e+\phi_0g_{0c}G_{cu}^e+\chi_3G_{cu}^e-\frac{1}{D_0}\,(G_c^e+\phi_0G_u^e)\,,\\ \mathcal{R}_{30}&\equiv g_{0c}F_{cc}^e+\phi_0\chi_3F_{uu}^e+\phi_0g_{0c}F_{cu}^e+\chi_3F_{cu}^e\,,\end{aligned} \tag{6.29 c}$$

where g_{0c}, χ_3, and ϕ_0, are defined in (6.25), (6.24 b), and (6.11), respectively. In addition, the coefficients $\mathcal{R}_{21}$ and $\mathcal{R}_{31}$ of the cubic term in (6.29 b) are given by

$$\begin{aligned}\mathcal{R}_{21}\equiv&\frac{1}{2}\left[G_{ccc}^e+G_{uuu}^e\phi_0^2\overline{\phi}_0+G_{ccu}^e\left(\overline{\phi}_0+2\phi_0\right)+G_{cuu}^e\left(\phi_0^2+2\phi_0\overline{\phi}_0\right)\right]\\ &+g_{0A}G_{cc}^e+\chi_6G_{cc}^e+\phi_0\chi_4G_{uu}^e+\overline{\phi_0}\chi_5G_{uu}^e+G_{cu}^e\left(\phi_0g_{0A}+\overline{\phi}_0\chi_6+\chi_4+\chi_5\right),\end{aligned} \tag{6.29 d}$$

and

$$\begin{aligned}\mathcal{R}_{31} \equiv \frac{1}{2}\left[F^e_{ccc} + F^e_{uuu}\phi_0^2\overline{\phi}_0 + F^e_{ccu}\left(\overline{\phi}_0 + 2\phi_0\right) + F^e_{cuu}\left(\phi_0^2 + 2\phi_0\overline{\phi}_0\right)\right] \\ + g_{0A}F^e_{cc} + \chi_6 F^e_{cc} + \phi_0\chi_4 F^e_{uu} + \overline{\phi_0}\chi_5 F^e_{uu} + F^e_{cu}\left(\phi_0 g_{0A} + \overline{\phi}_0\chi_6 + \chi_4 + \chi_5\right)\,.\end{aligned} \tag{6.29 e}$$

In (6.29 *d*) and (6.29 *e*), the quantities g_{0A}, χ_3, χ_4, χ_5, and χ_6 are defined in (6.25), (6.24 *b*), and (6.26 *b*).

The following lemma, consisting of a compatibility relation between $\mathcal{R}_1$, $\mathcal{R}_2$, and $\mathcal{R}_3$, provides a necessary condition for the existence of a solution to (6.28).

Lemma 6.1 *A necessary condition for (6.28) to have a solution is that $A(T)$ satisfies*

$$A'\left[\int_0^L \eta_0\overline{v}\,dx + \phi_0\overline{v}_1\right] = \frac{D_1}{D_0\tau}\left(1 + i\tau\lambda_I\right)A\int_0^L \eta_0\overline{v}\,dx + \overline{v}_1\mathcal{R}_3 - \mathcal{R}_2/\tau\,, \tag{6.30}$$

where $V \equiv (v, v_1)^T$ is the nontrivial solution, given in (6.19), to the homogeneous adjoint problem $\mathcal{L}^\star V = -i\lambda_I V$.

Proof: We define $U \equiv (\mathcal{C}_3, U_3)^T$, and we calculate from (6.28), and the definition of the inner product in (6.15), that

$$\langle \mathcal{L}U - i\lambda_I U\,, V\rangle = \int_0^L \mathcal{R}_1\overline{v}\,dx + \left(A'\phi_0 - \mathcal{R}_3\right)\overline{v}_1\,. \tag{6.31}$$

We then integrate by parts on the left-hand side of (6.31), and use the boundary conditions for v and $\mathcal{C}_3$ from (6.18) and (6.28 *b*), respectively. In this way, we obtain

$$\begin{aligned}\langle \mathcal{L}U - i\lambda_I U\,, V\rangle &= \int_0^L \left(\frac{D_0}{\tau}\overline{v}_{xx} - \frac{\overline{v}}{\tau}\right)\mathcal{C}_3\,dx + \left[F^e_c\mathcal{C}_3(0) + F^e_u U_3\right]\overline{v}_1 + \frac{D_0}{\tau}\left[\mathcal{C}_3(0)\overline{v}_x(0) - \mathcal{C}_{3x}(0)\overline{v}(0)\right] - i\lambda_I\langle U,\, V\rangle \\ &= \int_0^L \left(\frac{D_0}{\tau}\overline{v}_{xx} - \frac{\overline{v}}{\tau}\right)\mathcal{C}_3\,dx + \left(\overline{v}_1 F^e_u - \frac{1}{\tau}\overline{v}(0)G^e_u\right)U_3 - \frac{\overline{v}(0)}{\tau}\mathcal{R}_2 - i\lambda_I\langle U,\, V\rangle\,, \\ &= \langle U, \mathcal{L}^\star V + i\lambda_I V\rangle - \frac{\overline{v}(0)}{\tau}\mathcal{R}_2\,.\end{aligned} \tag{6.32}$$

To obtain the compatibility condition, we compare (6.31) with (6.32) and use $\mathcal{L}^\star V + i\lambda_I V = 0$. By substituting (6.29 *a*) for $\mathcal{R}_1$ into this condition, and recalling that $v(0) = 1$, we readily obtain (6.30). ■

Finally, upon substituting (6.29) into (6.30), we obtain the following amplitude equation for $A(T)$:

$$A' = D_1 b_1 A + b_2 A^2\overline{A}\,, \tag{6.33 a}$$

where the complex-valued coefficients b_1 and b_2, which are independent of D_1, are given by

$$b_1 \equiv \frac{1}{\mathcal{N}}\left[\frac{(1 + i\tau\lambda_I)}{D_0\tau}\int_0^L \eta_0\overline{v}\,dx + \overline{v}_1\mathcal{R}_{30} - \mathcal{R}_{20}/\tau\right]\,, \qquad b_2 \equiv \frac{1}{\mathcal{N}}\left[\overline{v}_1\mathcal{R}_{31} - \mathcal{R}_{21}/\tau\right]\,, \tag{6.33 b}$$

where we have defined $\mathcal{N}$ by

$$\mathcal{N} \equiv \left[\int_0^L \eta_0\overline{v}\,dx + \phi_0\overline{v}_1\right]\,. \tag{6.33 c}$$

In (6.33 *b*), the coefficients $\mathcal{R}_{20}$, $\mathcal{R}_{30}$, $\mathcal{R}_{21}$, and $\mathcal{R}_{31}$, are defined in (6.29 *c*), (6.29 *d*), and (6.29 *e*). Moreover, $v(x)$ and v_1 are the components of the adjoint eigenfunction V, satisfying $\mathcal{L}^\star V = -i\lambda_I V$, given in (6.19).

The ODE (6.33 *a*), commonly referred to as the Stuart-Landau equation, characterizes the weakly nonlinear behavior of the oscillation near the critical stability threshold. We write A as $A = re^{i\theta}$ and decompose b_1 and b_2 into real and imaginary parts as $b_1 = b_{1R} + ib_{1I}$ and $b_2 = b_{2R} + ib_{2I}$. From (6.33 *a*), we obtain that r and θ satisfy

$$r' = r\left(D_1 b_{1R} + b_{2R}r^2\right)\,, \qquad \theta' = D_1 b_{1I} + b_{2I}r^2\,. \tag{6.34}$$

The fixed points in r, when they exist, correspond to periodic solutions for A. These special solutions are

$$r_e = \sqrt{-\frac{b_{1R}D_1}{b_{2R}}}\,; \qquad \theta = \tilde{\theta}T\,, \qquad \tilde{\theta} \equiv D_1 b_{1I} + b_{2I} r_e^2\,. \tag{6.35}$$

For $\epsilon \to 0$, and with $D - D_0 = \epsilon^2 D_1$, we conclude from (6.4), (6.9), and (6.35), that there is a periodic solution near the Hopf bifurcation point of the form

$$\begin{pmatrix} C(x,t,T) \\ u(t,T) \end{pmatrix} \sim \begin{pmatrix} C_e(x) \\ u_e \end{pmatrix} + \epsilon \left[r_e e^{i(\lambda_I + \epsilon^2\tilde{\theta})t} \begin{pmatrix} \eta_0(x) \\ \phi_0 \end{pmatrix} + \text{c.c.} \right]. \tag{6.36}$$

The analysis of the amplitude equation (6.34) is routine, and depends on the signs of b_{1R} and b_{2R}. The Hopf bifurcation is supercritical when $b_{2R} < 0$ and is subcritical if $b_{2R} < 0$. More precisely, if $b_{1R} > 0$, the symmetric steady-state solution $(C_e(x),\, u_e)$ is linearly stable if $D_1 < 0$ and is unstable if $D_1 > 0$. An unstable branch of periodic solutions exists in the region $D_1 < 0$ if $b_{2R} > 0$ (subcritical Hopf). If $b_{2R} < 0$, then there is a stable periodic solution branch in the region $D_1 > 0$ (supercritical Hopf). In contrast, if $b_{1R} < 0$, the symmetric steady-state solution $(C_e(x),\, u_e)$ is linearly stable if $D_1 > 0$ and is unstable if $D_1 < 0$. An unstable branch of periodic solutions exists in the region $D_1 > 0$ if $b_{2R} > 0$ (subcritical Hopf). If $b_{2R} < 0$, there is a stable periodic solution branch for $D_1 < 0$ (supercritical Hopf).

Remark 6.1 *A similar weakly nonlinear analysis can be done to determine whether an asynchronous periodic solution branch is subcritical or supercritical at the Hopf bifurcation point. To consider this case, we simply replace the no-flux condition at $x = L$ for $\eta(x)$, $v(x)$, and $C_j(x)$ for $j = 1, \ldots, 3$ with a homogeneous Dirichlet condition. We do not carry out the details of this calculation here.*

6.1 Numerical Validation of the Weakly Nonlinear Theory

We now apply our weakly nonlinear theory to the explicitly solvable model system of §4.2, where $G(C(0,t),u)$ and $F(C(0,t),u)$ are given in (4.6). Since, for this example, $F(C(0,t),u)$ is linear in its variables, the only nonlinearity in (6.1) arises from $G(C(0,t),u)$. In our analysis, we will focus on periodic solutions that bifurcate from the steady-state solution branch where $C_e^0 \equiv C_e(0)$ is positive, and given explicitly in (4.8). For this system we compare predictions from the amplitude equation (6.33) with full numerical results computed from the numerical bifurcation software XPPAUT (cf. [**6**]). The numerical procedure used to compute these bifurcation diagrams is described in §4.

Treating D as the main bifurcation parameter we numerically computed steady-state and periodic solution branches of (6.1) for two values of γ. In our numerical experiments, we found that a periodic solution bifurcates via a Hopf bifurcation from the positive steady-state solution branch. As shown in Fig. 12, by tuning the parameter γ, while holding the other parameters fixed, the Hopf bifurcation was found to change from supercritical to subcritical.

By using the amplitude equation (6.33), our weakly nonlinear asymptotic theory predicts that the switching point from a supercritical to a subcritical Hopf bifurcation occurs at $\gamma = 1.628$ (accurate to three decimal places), which agrees with the corresponding numerical result. Furthermore, the amplitude equation also allow us to approximate the solution near the Hopf bifurcation point as shown in (6.36). For the local variable $u(t)$, we obtain from (6.36) that the amplitude of the periodic solution can be written as

$$|u(t,T) - u_e| = \epsilon r_e |e^{i(\lambda_I + \epsilon^2\tilde{\theta})t}\phi_0 + \text{c.c.}| = 2\epsilon r_e |\phi_0|\,, \tag{6.37}$$

where r_e is the fixed point of the amplitude equation given in (6.35). Here $\epsilon \ll 1$ and ϕ_0 is the eigenfunction of $u(t)$,

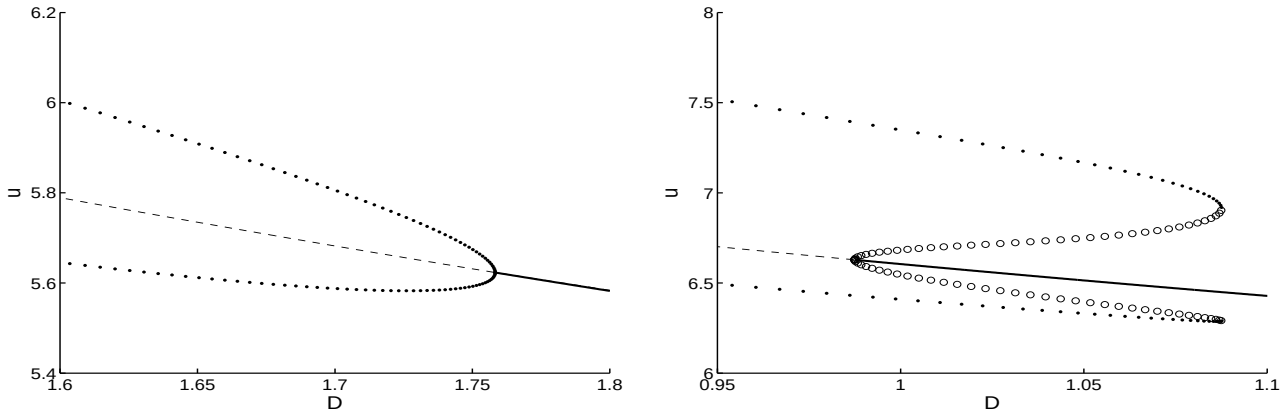

Figure 12. Bifurcation diagrams with diffusivity D as bifurcation parameter showing either a supercritical or subcritical Hopf bifurcation structure for (6.1), with coupling functions given in (4.6), for two values of γ. Left panel: $\gamma = 1.55$ (supercritical). Right panel: $\gamma = 1.7$ (subcritical). The solid and dashed lines denote stable and unstable steady-state solutions, respectively. Open circles indicate the max/min amplitude of unstable periodic solutions, while the solid dots correspond to linearly stable periodic solution branches. The bulk diffusion parameters are $\tau = 0.1$ and $L = 5$. The membrane kinetic and coupling parameters are $\beta = 1$ and $\kappa = 12$.

given explicitly in (6.11). If we define $u_{\rm amp} \equiv |u(t,T) - u_e|$ and plot $\pm u_{\rm amp}$ versus the diffusivity D, then $u_{\rm amp}$ should be proportional to $\epsilon \equiv \sqrt{D - D_0}$ in the vicinity of the Hopf bifurcation point D_0. The quantity $u_{\rm amp}$ is plotted in Fig. 13.

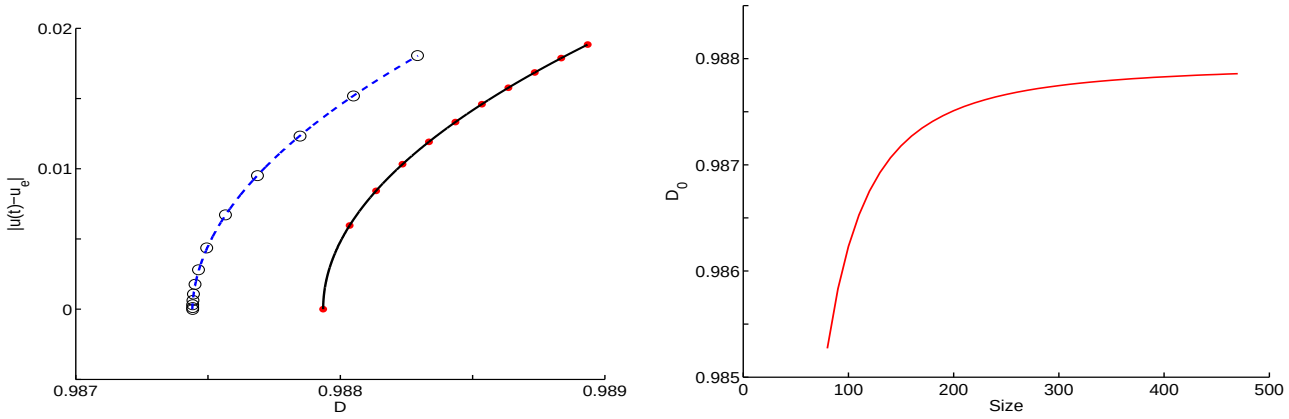

Figure 13. Left panel: Comparison of bifurcation diagrams near a subcritical Hopf bifurcation obtained from the bifurcation software XPPAUT and from the weakly nonlinear analysis. Red dots indicate the amplitude of the unstable periodic solution $u_{\rm amp}$ (see the text) obtained from the amplitude equation (6.33) and the black circles are from the bifurcation software. The black and blue curves are the corresponding fitted parabola and the curvature of the two curves are 5.6 (black) and 5.0 (blue), respectively, at the Hopf bifurcation point $D_0 = 0.9879$ (red dots) and $D_0 = 0.9874$ (black circles). The computations are done with 80 interior spatial meshpoints. Right panel: Plot of the Hopf bifurcation point D_0 versus the number of spatial meshpoints of the discretized system. The parameter values are the same as those used in Fig. 12 with $\gamma = 1.7$.

The left panel of Fig. 13 shows a comparison between the analytical and numerical bifurcation diagrams near a subcritical Hopf bifurcation point D_0. In our numerical experiments, since we discretized the PDE-ODE system (6.1), with coupling functions (4.6), with finite differences into a system of ODEs, some error is incurred in predicting the location of the Hopf bifurcation value D_0. In contrast, in the implementation of the weakly nonlinear theory we solved the transcendental equation (6.12) for a complex conjugate pair of imaginary eigenvalues and D_0 directly. Therefore, the D_0 calculated

from (6.12) is more accurate than the one computed from the numerics and it results in the shifting of the bifurcation point D_0, as shown in the left panel of Fig. 13. The right panel of Fig. 13 shows how the numerically calculated value D_0 shifts towards the more accurate value, computed from (6.12), when we increase the number of spatial meshpoints in the discretized system. Although, there is a small difference in predicting the value of D_0, the amplitude calculated by the weakly nonlinear theory shows good agreement with the corresponding amplitude computed from the numerical bifurcation software, as evidenced by the close comparison of the curvature of the two curves in Fig. 13 at $D = D_0$.

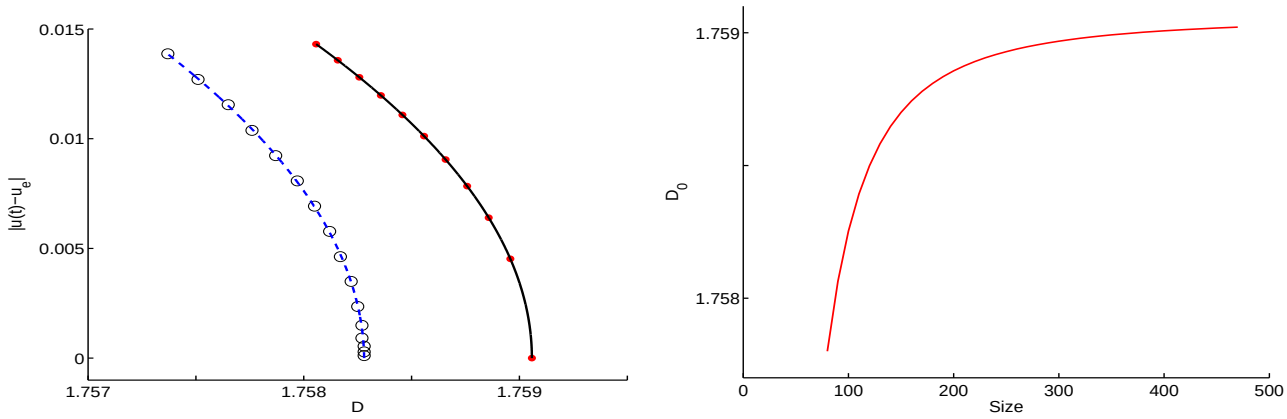

Figure 14. Left panel: Comparison of bifurcation diagrams near a supercritical Hopf bifurcation obtained from the bifurcation software XPPAUT and from the weakly nonlinear analysis. The notations are the same as those in Fig. 13 except now the red dots and black circles denote the stable periodic solution branch. The curvature of the two curves are 9.8 (black) and 9.3 (blue), respectively, at the Hopf bifurcation point $D_0 = 1.7591$ (red dots) and $D_0 = 1.7583$ (black circles). The computations are done with 80 interior spatial meshpoints. Right panel: Plot of the Hopf bifurcation point D_0 versus the number of spatial meshpoints of the discretized system. The parameter values are the same as those used in Fig. 12 with $\gamma = 1.55$.

Fig. 14 compares the numerical bifurcation diagram with the asymptotic prediction near a supercritical Hopf bifurcation point D_0. The amplitude of the stable periodic orbits calculated by the weakly nonlinear theory and the numerical simulations are seen to compare favorably. The right panel of Fig. 14 shows that the numerically calculated Hopf bifurcation point shifts toward the more accurate value as the number of interior meshpoints increase.

7 Discussion

On a one-dimensional spatial domain, we have introduced and analyzed a class of models that couple two dynamically active membranes, separated spatially by a distance $2L$, through a linear bulk diffusion field. For this class of models, we have shown both analytically and numerically that bulk diffusion can trigger a stable synchronous oscillatory instability in the temporal dynamics associated with the two active membranes.

There are many open problems in this direction that warrant further study. One main direction is to consider more thoroughly the case of multi-species membrane dynamics. More specifically, although a numerical winding number computation is readily implemented for multi-species membrane dynamics, there is a need to extend the theoretical spectral results of §3.1 to the case of more than a single membrane-bound species (see §5 for an example of a two-species dynamics). Furthermore, it would be interesting to extend the weakly nonlinear analysis of §6 to the case of multiple membrane-bound species. It would also be scientifically relevant to both formulate and analyze related PDE-ODE models, where the membrane-bulk coupling strength can vary dynamically, so as to create periodic bursts of synchronous oscillatory

behavior, followed by intervals of quiescent behavior, in the two membranes. Triggered oscillations and bursters due to slowly varying external or internal parameters have been well-studied in a purely ODE context (cf. [**1**], [**2**], [**15**], [**20**]).

A second open direction, amenable to a numerical bifurcation approach, would be to study the linear stability of bifurcating branches of synchronous and asynchronous periodic solutions, and to explore any secondary instabilities emanating from these branches. For our examples of one-species membrane dynamics, the bifurcating synchronous solution branch in Fig. 3 (see also Fig. 8) has a rather large parameter range of stability. Can these observations be made into a more general statement for other coupled membrane-bulk models? For a specific two-component coupled membrane-dynamics with Selkov kinetics, it has been shown that synchronous and asynchronous oscillations can each undergo an exchange of stability at the same parameter set (cf. [**12**]). In [**12**], an analytical theory to examine oscillatory dynamics near such a co-dimension-2 bifurcation was given. In addition, for a two-species membrane dynamics, as shown in the left panel of Fig. 9, there can be secondary instabilities off of the primary periodic solution branches, and the global bifurcation structure is much more complicated. It would be interesting to explore these issues numerically, with an aim of potentially discovering whether there can be any period-doubling route to chaotic dynamics such as was observed computationally in [**22**] for a related model consisting of a linear RD system with nonlinear fluxes at fixed lattice sites.

A further open direction relates to our assumption that the bulk diffusion field has a constant diffusivity and undergoes a linear bulk degradation. It would be worthwhile to extend our analysis to allow for either a nonlinear degradation of the signaling molecule in the bulk, a nonlinear diffusivity, or to allow for a sub-diffusive bulk diffusion process. Either of these three additional effects could be important in various biological applications.

Finally, an extension of our analysis to the case of multiple spatial dimensions, such as where reaction dynamics can occur either on closed surfaces, or within localized compartments, should be undertaken.

Acknowledgements

Y. X. Li, W. Nagata, and M. J. Ward acknowledge the grant support from NSERC (Canada). We are grateful to Prof. Pik-Yin Lai (Taiwan), Prof. Thomas Erneux (U. Brussels), and Prof. Bard Ermentrout (U. Pittsburgh) for sharing their insights with us on membrane-bulk dynamics.

Appendix A Two Specific Biological Models

The Dictyostelium Model

The amoeba *Dictyostelium discoideum* is one of the most studied organism in biology. There are many stages in the life cycle of each such amoeba cell. When nutrient is readily available, they live as single cell organisms. However, when food becomes scarce, each cell starts to release cyclic AMP (cAMP) in order to attract other cells, and at the same time themselves are attracted by the cAMP signal emitted by others. This secretion results in an aggregation of individual amoeba to form aggregate centers [**9**]. This intercellular communication mechanism presents some similarities with the endocrine system in higher organisms. In [**9**] a two-variable model was proposed to describe the cAMP (cyclic adenosine monophosphate) oscillations in Dictyostelium cells. This minimal model was obtained from a reduction of a more elaborate model based on desensitization of the cAMP receptor which consists of variables representing molecules such as the active(R) and desensitized(D) forms of the receptor, free(C) and active form(E) of adenylate cyclase, intracellular(P_i) and extracellular(P) cAMP, and substrate ATP(S). In [**9**] this minimal model was used to analyze the bursting and birhythmicity observed in experiments with amoeba cells. The model is formulated as

$$\frac{d\rho_t}{dt} = f_2(\gamma) - \rho_t(f_1(\gamma) + f_2(\gamma))\,, \qquad \frac{d\gamma}{dt} = \sigma^*\psi(\rho_t,\gamma) - k_e\gamma\,, \tag{A.1 a}$$

where

$$f_1(\gamma) \equiv \frac{k_1 + k_2\gamma^2}{1+\gamma^2}\,, \qquad f_2(\gamma) \equiv \frac{k_1 L_1 + k_2 L_2 c_d^2 \gamma^2}{1 + c_d^2\gamma^2}\,, \qquad \psi(\rho_t,\gamma) \equiv \frac{\alpha\left(\Lambda\theta + \frac{\epsilon\rho_t\gamma^2}{1+\gamma^2}\right)}{(1+\alpha\theta) + \left(\frac{\epsilon\rho_t\gamma^2}{1+\gamma^2}\right)(1+\alpha)}\,. \tag{A.1 b}$$

Here ρ_t is the total fraction of receptor in the active state, α and γ denote the normalized concentration of intracellular ATP and extracellular cAMP, θ is the ratio of Michaelis constants for the E and C forms of adenylate cyclase, Λ is the ratio of catalytic constants of forms C and E of adenylate cyclase, ϵ is the coupling constant for activation of C by cAMP-receptor complex in active state, k_1 is the rate constant for the modification step from R to D, L_1 is the equilibrium ratio of the states R and D, k_2 is the rate constant for modification step from R to D in the presence of cAMP, L_2 is the corresponding equilibrium ratio, k_e is the ratio of maximum activity for extracellular phosphodiestease and the Michaelis constant of extracellular phosphodiesterase for cAMP, c_d is the ratio of dissociation constants of cAMP-receptor complex in R and D states, σ^* is calculated as some combination of other constants. For a more detailed discussion of this model see [**9**] (pp. 195–258).

Since the cAMP molecules can diffuse in space, in our model we assume that the extracellular cAMP is also a function of location, so that $\gamma = \gamma(x,t)$. We assume that it can diffuse freely in space, with some bulk decay, but that all the reactions occur on the boundaries of amoeba cells. In this way, our model for cAMP, given a cell at $x = 0$ and at $x = 2L$, and with $\tau \equiv 1/k_e$ is

$$\begin{aligned} &\tau\frac{d\gamma}{dt} = D\frac{d^2\gamma}{dx^2} - \gamma\,, \qquad t>0\,, \quad 0<x<L\,; \qquad \gamma_x(L,t) = 0\,, \qquad D\gamma_x(0) = -\sigma^\star\psi(\rho_t,\gamma(0,t))\,, \\ &\frac{d\rho_t}{dt} = f_2(\gamma(0,t)) - \rho_t\left[f_1(\gamma(0,t)) + f_2(\gamma(0,t))\right]\,. \end{aligned} \tag{A.2}$$

The GnRH Model

Gonadotropin-releasing hormone (GnRH) is a decapeptide secreted by GnRH neurons in the hypothalamus that regulates the reproductive function in mammals. There are about 800-2000 GnRH neurons scattered in a few areas of the hypothalamus. Each GnRH neuron releases GnRH to portal blood in an oscillatory profile with a period of several minutes and they synchronize to produce large GnRH pulses with a period ranging from twenty minutes to one hour. Experiments reveal that GnRH neurons express GnRH receptors. Based on these biological facts, a possible synchronization mechanism of GnRH neurons was proposed in [**19**, **7**, **13**]. In this model, it is assumed the the GnRH neurons are coupled through GnRH in the extracellular environment. This model was able to predict that oscillations occur over a one hour period. Assuming two neurons, one each at $x = 0$ and at $x = 2L$, this model system is

$$g_t = Dg_{xx} - g\,, \qquad t>0\,, \quad 0<x<L\,; \qquad g_x(L,t) = 0\,, \quad Dg_x(0) = -\sigma j\,, \tag{A.3 a}$$

with the three-component membrane dynamics

$$\alpha_t = \phi_\alpha\left(\frac{[g(0,t)]^{n_\alpha}}{k_\alpha^{n_\alpha} + [g(0,t)]^{n_\alpha}}\,, \alpha\right)\,, \qquad \alpha = \{s,q,i\}\,. \tag{A.3 b}$$

with coefficients $n_s = 4$, $n_q = 2$ and $n_i = 2$. In (A.3 *a*), σ reflects the secretion efficiency, and the boundary flux is

$$j \equiv 1 + \beta\left(\frac{\iota + 1 + \zeta q}{\mu + 1 + \delta q}\right)^3\left(\eta + \frac{s}{\omega + i}\right)^3\,, \tag{A.3 c}$$

(see [**19**, **13**] for further details and definition of the parameters). In (A.3 *a*), s, q and i denote the concentration of three G-proteins, G_S, G_Q and G_I, respectively. It is postulated that the release of GnRH is mediated through activation (G_S, G_Q) and inhibition (G_I) of these proteins. With the assumption that the time scales of s and q are much faster than i, we use a quasi-steady state approximation to fix s and q at (approximately) their steady-state values. This leads to the

following reduced coupled system

$$g_t = Dg_{xx} - g\,, \qquad t > 0\,, \quad 0 < x < L\,; \qquad g_x(L,t) = 0\,, \quad Dg_x(0) = G\left(g(0,t), i\right)\,, \tag{A.4 a}$$

with the one-component membrane dynamics and boundary flux given by

$$i_t = \epsilon\left(\frac{[g(0,t)]^2}{k_i^2 + [g(0,t)]^2} - i\right)\,, \qquad G\left(g(0,t), i\right) = -\sigma\left[1 + \beta\left(\frac{\iota + 1 + \zeta q}{\mu + 1 + \delta q}\right)^3\left(\eta + \frac{s}{\omega + i}\right)^3\right]\,, \tag{A.4 b}$$

Here, s and q, which depend on $g(0,t)$, are given by

$$s = \frac{[g(0,t)]^4}{k_s^4 + [g(0,t)]^4}\,, \qquad q = \frac{[g(0,t)]^2}{k_q^2 + [g(0,t)]^2}\,. \tag{A.4 c}$$

References

[1] S. M. Baer, T. Erneux, J. Rinzel, *The Slow Passage Through a Hopf bifurcation: Delay, Memory Effects, and Resonance*, SIAM J. Appl. Math., **49**(1), (1989), pp. 5571.

[2] R. Bertram, M. J. Butte, T. Kiemel, A. Sherman, *Topological and Phenomenological Classification of Bursting Oscillations*, Bull. Math. Bio. **57**(3), (1995), pp. 413–439.

[3] W. Y. Chiang, Y. X. Li, P. Y. Lai, *Simple Models for Quorum Sensing: Nonlinear Dynamical Analysis*, Phys. Rev. E., **84**, (2011), 041921.

[4] T. Chou, M. R. D'Orsogna, *Multistage Adsorption of Diffusing Macromolecules and Viruses*, J. Chem. Phys., **127**(1), J. Chem. Phys., (2007), 105101.

[5] J. Ding, A. Zhu, *Eigenvalues of Rank-One Updated Matrices with Some Applications*, Appl. Math Lett., **20**(12), (2007), pp. 1223-1226.

[6] G. B. Ermentrout, *Simulating, Analyzing, and Animating Dynamical Systems: A Guide to XPPAUT for Researchers and Students*, SIAM 2002, Philadelphia, USA.

[7] P. A. Fletcher, Y. X. Li, *An Integrated Model of Electrical Spiking, Bursting, and Calcium Oscillations in GnRH Neurons*, Biophysical J., **96**(11), (2009), pp. 4514–4524.

[8] B. Friedman, *Principles and Techniques of Applied Mathematics*, Applied Mathematics Series, John Wiley, New York, (1956), 315 pp.

[9] A. Goldbeter, *Biochemical Oscillations and Cellular Rhythms: The Molecular Bases of Periodic and Chaotic Behaviour*, Cambridge U. Press, Cambridge, U.K. (1990), 632 pp.

[10] A. Gomez-Marin, J. Garcia-Ojalvo, J. M. Sancho, *Self-Sustained Spatiotemporal Oscillations Induced by Membrane-Bulk Coupling*, Phys. Rev. Lett., **98**(16), (2007), 168303.

[11] J. Gou, M. J. Ward, *Oscillatory Dynamics for a Coupled Membrane-Bulk Diffusion Model with Fitzhugh-Nagumo Kinetics*, submitted, SIAM J. Appl. Math., (June 2015), (23 pages).

[12] J. Gou, Y. X. Li, W. Nagata, *Interactions of In-Phase and Anti-Phase Synchronies in Two Cells Coupled by a Spatially Diffusing Chemical: Double-Hopf Bifurcations*, submitted, IMA J. Appl. Dyn. Syst., (July 2015), (23 pages).

[13] A. Khadra, Y. X. Li, *A Model for the Pulsatile Secretion of Gonadotrpin-Releasing Hormone from Synchronized Hypothalamic Neurons*, Biophysical J., **91**(1), (2006), pp. 74–83.

[14] B. N. Kholodenko, *Cell-Signalling Dynamics in Time and Space*, Nat. Rev. Mol. Cell Biol., **7**, (2006), pp. 165–176.

[15] C. Kuehn, *A Mathematical Framework for Critical Transitions: Bifurcations, Fast/Slow systems and Stochastic Dynamics*, Physica D, **240**(12), (2011), pp. 1020–1035.

[16] P. Y. Lai, *private communication*, (2013).

[17] H. Levine, W. J. Rappel, *Membrane Bound Turing Patterns*, Phys. Rev. E., **72**, (2005), 061912.

[18] C. Levy, D. Iron, *Dynamics and Stability of a Three-Dimensional Model of Cell Signal Transduction*, Journ. Math. Bio., **67**(6-7), (2013), pp. 1691–1728.

[19] Y. X. Li, A. Khadra, *Robust Synchrony and Rhythmogenesis in Endocrine Neurons via Autocrine Regulations in Vitro and in Vivo*, Bull. Math. Biology, **70**(8), (2008), pp. 2103–2125.

[20] P. Mandel, T. Erneux, *The Slow Passage Through a Steady Bifurcation: Delay and Memory Effects*, J. Stat. Physics, **48**(5-6), (1987), pp. 1059–1070.

[21] J. Müller, H. Uecker, *Approximating the Dynamics of Communicating Cells in a Diffusive Medium by ODEs - Homogenization with Localization*, J. Math. Biol., **67**(5), (2013), pp. 1023–1065.

[22] F. Naqib, T. Quail, L. Musa, H. Vulpe, J. Nadeau, J. Lei, L. Glass, *Tunable Oscillations and Chaotic Dynamics in Systems with Localized Synthesis*, Phys. Rev. E., **85**, (2012), 046210.

[23] Y. Nec, M. J. Ward, *An Explicitly Solvable Nonlocal Eigenvalue Problem and the Stability of a Spike for a Sub-Diffusive Reaction-Diffusion System*, Math. Modeling Natur. Phen., **8**(2), (2013), pp. 55–87.
[24] B. Novák, J. J. Tyson, *Design Principles of Biochemical Oscillators*, Nature Rev. Mol. Cell. Bio., **9**(12), (2008), pp. 981–991.
[25] A. P. Peirce, H. Rabitz, *Effect of Defect Structures on Chemically Active Surfaces: A Continuum Approach*, Phys. Rev. B., **38**(3), (1998), pp. 1734–1753.
[26] J. A. Pelesko, *Nonlinear Stability Considerations in Thermoelastic Contact*, ASME Journal Appl. Mech., **66**(1), (1999), pp. 109–116.
[27] J. A. Pelesko, *Nonlinear Stability, Thermoelastic Contact, and the Barber Condition*, ASME Journal Appl. Mech., **68**(1), (2001), pp. 28–33.
[28] S. Y. Shvartsman, E. Schütz, R. Imbihl, I. G. Kevrekidis, *Dynamics on Microcomposite Catalytic Surfaces: The Effect of Active Boundaries*, Phys. Rev. Lett., **83**, (1999), 2857.
[29] M. J. Ward, J. Wei, *Hopf Bifurcations and Oscillatory Instabilities of Spike Solutions for the One-Dimensional Gierer-Meinhardt Model*, J. Nonlinear Science, **13**(2), (2003), pp. 209–264.